

Investigation of the luminescence of $[\text{UO}_2\text{X}_4]^{2-}$ ($\text{X}=\text{Cl}, \text{Br}$) complexes in organic phase using time-resolved laser-induced fluorescence spectroscopy and quantum chemical simulations

Hanna Oher and Thomas Vercouter

*DEN-Service d'Etudes Analytiques et de Réactivité des Surfaces (SEARS),
CEA, Université Paris-Saclay, F-91191 Gif-sur-Yvette, France**

Florent Réal and Valérie Vallet

Univ. Lille, CNRS, UMR 8523 - PhLAM - Physique des Lasers Atomes et Molécules, F-59000 Lille, France

The luminescence properties of the $[\text{UO}_2\text{Cl}_4]^{2-}$ complex in an organic phase, especially the influence of large organic counter cations, have been studied by time-resolved laser-induced fluorescence spectroscopy (TRLFS) and *ab initio* modeling. The experimental spectrum was assigned by vibronic Franck-Condon calculations on quantum chemical methods on the basis of a combination of relativistic density functional approaches. The shape of the luminescence spectrum of the uranyl tetrachloride complex is determined by symmetrical vibrations and geometrical change upon emission. The possible change in the luminescence properties depending on the first and second uranyl coordination spheres was predicted theoretically for the $[\text{UO}_2\text{Br}_4]^{2-}$ and $[\text{R}_4\text{N}]_2[\text{UO}_2\text{Cl}_4]$ ($[\text{R}_4\text{N}] = [\text{Bu}_4\text{N}], [\text{A336}]$) systems. The computations reveal that for U(VI), the second coordination sphere has little influence on the spectrum shape, making speciation of uranyl complexes with identical first coordination-sphere ligands tedious to discriminate. The computed structural changes agreed well with experimental trends; theoretical spectra and peak attributions are in a good accordance with TRLFS and magnetic circular dichroism (MCD) data respectively.

I. INTRODUCTION

The knowledge of the stoichiometries and stabilities of the chemical species of uranium is of key importance for an understanding of the chemical reactivity of uranium in environmental or industrial situations. The speciation of uranium in solution has thus been a major topic of investigations by both experimental and theoretical methods. Among the powerful spectroscopic techniques, time-resolved laser-induced luminescence spectroscopy (TRLFS) has been widely used for the characterization of uranyl species in solutions and in solid phases, because of its high sensitivity to changes in the first coordination sphere of UO_2^{2+} . The luminescence spectra of uranyl complexes in solution show in general a narrow energetic range of about 6000 cm^{-1} . In this region only a single electronic transition between the initial and final states can be identified and it is vibrationally resolved with the bands corresponding to different vibrational quantum numbers [1]. In the case of mixtures of uranyl species, the interpretation of TRLFS data can be difficult as one needs to deconvolute overlapping emission spectra in similar time frames. Therefore, spectroscopic considerations are often insufficient to unambiguously determine the nature of the complexes. This is why a theoretical support based on quantum chemical modeling appears as a way to better validate TRLFS data interpretations by decomposing the different effects that might induce changes in the emission spectra of uranyl complexes.

Several research teams have tried to simulate emission spectra of uranyl complexes with quantum chemical methods [2–4], on the basis of either wave-function theory (WFT) or density functional theory (DFT) and by taking into account relativistic effects [5–8] (scalar relativistic effects and spin-orbit coupling), as they are important for actinide complexes. While WFT methods are well-suited for accurate calculations, the high computing costs limit the simulations to small clusters of heavy elements such as uranium. DFT approaches are more appropriate for cost-effective calculations applied to actinides but can be challenging with regard to their accuracy for the description of the electronic ground and excited states and their ability to reproduce low-lying electronic transitions and their vibronic resolutions. Tecmer et al. [9] have evaluated the accuracy of pure and hybrid exchange-correlation functionals for the bare uranyl cation isoelectronic uranium triatomics, arguing that hybrid functionals can be used for quantitative prediction of the low-lying excited states of uranyl. Uranyl tetrachloride complexes have been thoroughly studied as a reference system because direct comparisons with luminescence data from crystals are possible [10]. Moreover, this complex can also be stabilized in nonaqueous solvents [11–13] and is of interest in some solvent extraction protocols [14, 15]. The structure of the uranyl tetrachloride is well-established, with four chloride ions in the equatorial plane of the UO_2^{2+} moiety, resulting in a D_{4h} symmetry. The effects of second-sphere counterions, solvent molecules, or solvating agents also have to be considered, in order to quantify their influence on the structures, the electronic state energies, and the vibronic progressions.

In this work we compare the results of *ab initio* calculations to experimental data obtained from a *n*-dodecane

* Univ. Lille, CNRS, UMR 8523 - PhLAM - Physique des Lasers Atomes et Molécules, F-59000 Lille, France

solution in which the uranyl tetrachloride complex was extracted by a tetraalkylammonium molecule (Aliquate[®] 336). The methodology is a step-by-step approach in order to validate the hypotheses and approximations we made. The computations of the ground and the excited state structural and vibrational parameters are necessary for an understanding of the theoretical and experimental spectra. Because the main effect on the luminescence data is commonly accepted to originate from the first coordination sphere, the chloride ligands were substituted by bromides to discuss the trends, validate our method, and evaluate its applicability to other types of uranyl complexes. We will also quantify the effects of outer-sphere counterions and long-range solvation effects on the computed spectra.

II. EXPERIMENTAL AND COMPUTATIONAL DETAILS

A. Sample Preparation: [A336]₂[UO₂Cl₄] in *n*-Dodecane

The sample preparation method has been adapted from Hellé et al. [15, 16]. Aliquate[®] 336 (98 %) was purchased from Alfa Aesar. HCl (32 %), 1-decanol (99 %) and *n*-dodecane were purchased from Sigma-Aldrich. HClO₄ was purchased from Merck. All reagents were used as received without further purification. A stock solution of uranium(VI) was prepared by dissolution of U₃O₈ in a hot perchloric acid solution. The U(VI) concentration was checked by inductively coupled plasma mass spectrometry (ICP-MS). The aqueous solution was prepared by dilution of this stock solution into a 5 M hydrochloric acid solution to get a uranium (VI) concentration of 10⁻⁵ M. Deionized water (Alpha-Q, Millipore, 18.2 MΩcm) was used for the preparation of all aqueous solutions.

The organic solution was prepared by dissolving weighed amounts of Aliquate[®] 336 and 1-decanol in sufficient amount of *n*-dodecane to reach a concentration of 10⁻² M of Aliquate[®] 336 with 1 % of 1-decanol. It was then pre-equilibrated by contact with a uranium-free 5 M hydrochloric acid solution during 2 h of shaking and separated.

For uranium extraction, 2 mL of the aqueous solution was contacted with an equal volume of the pre-equilibrated organic solution. The mixture was shaken in a thermomixer at 20 °C during 1 h, and about 2 mL of the organic phase was sampled after 2 h of decantation for the spectroscopic measurements.

B. Time-Resolved Laser-Induced Fluorescence Spectroscopy

The sample was put in a 1 cm path length quartz cuvette that was placed in a TR-LFS setup as described afterward. The excitation wavelength was provided by a tunable OPO system (PantherEx OPO, Excel Technology) pumped by a Nd/YAG laser at 355 nm (Surelite-I,

Excel Technology). The excitation was tuned to $\lambda_{ex} = 427$ nm which corresponds to a maximum of absorption by uranium(VI) in our samples. The 5 ns laser pulses were generated at 10 Hz for an energy of about 3.15 mJ. The detection setup has already been described elsewhere [17]. The luminescence signal was collected during a gate width of 200 μ s, with a gate delay of 100 ns after the excitation by the laser pulse, the delay value being carefully chosen as discussed in the Supporting Information. The luminescence spectrum of the sample was recorded at room temperature ((22 \pm 1) °C) from the accumulation of 1000 scans. The background noise was subtracted by the software from the recorded spectrum of a [A336]₂[UO₂Cl₄] in *n*-dodecane sample.

C. Computational Details

Since our aim is to use quantum chemical methods to elucidate the luminescence band shapes of the complexes, several data need to be calculated. The ground-state and first-excited-state geometries, their associated harmonic frequency spectra, and Hessian matrices have to be computed in order to derive the overlap integrals between the vibrational wave-functions associated with the ground and excited states - Franck-Condon factors (FCFs). The FCFs were computed using the ezSpectrum 3.0 [18] program by taking all necessary data generated by the ab initio packages described below. The Duschinsky rotations were used as implemented in the program. The numbers of vibrational quanta in excited and ground state were selected to be one and five, respectively. All of the spectra were computed at 300 K. For the larger systems, all normal modes with vibrational frequencies larger than 1000 cm⁻¹ were excluded from the FCF calculations, to keep the computational costs affordable.

a. Model Systems. The interactions between uranyl and its first and second coordination spheres might affect the electronic structure of the uranyl unit. As the influence of the chloride ligands in the UO₂Cl₄²⁻ complex was excellently reviewed by different experimental [11, 12, 19–21] and theoretical methods [22–26], this system was selected as a benchmark to quantify the effect of ligands in the first coordination sphere by substituting chlorides with bromides and the effect of the counterions in the second coordination sphere: i.e., the quaternary ammonium cations. Furthermore, to discuss the importance of long-range solvent effects, the model systems were computed in the gas phase and with inclusion of solvent effects (*n*-dodecane and acetone). The structures are represented in Fig. 1

b. Structures of the Ground and Excited states and Harmonic Frequencies. For the sake of keeping the computational costs within a scale of 1 week and of simplifying the data analysis, the structures of the uranyl tetrahalide complexes were enforced to have *D*_{4h} symmetry, whereas no symmetry constraints were applied to the complexes with a second coordination sphere. All

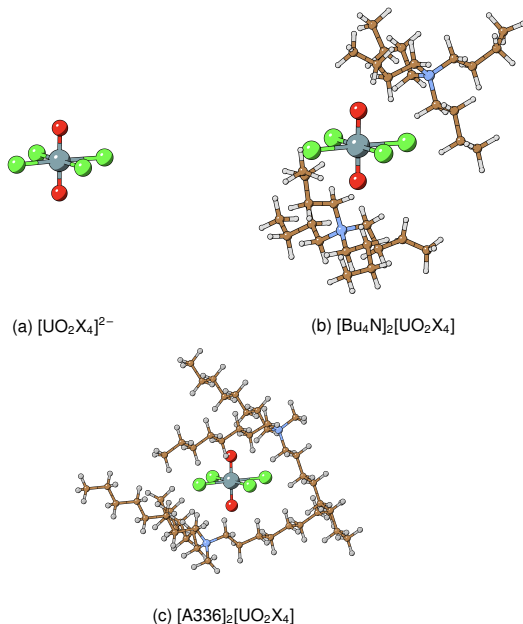


FIG. 1: Structures of $[R_4N]_2[UO_2X_4]$ complexes ($[R_4N] = [Bu_4N], [A336]$; $X=Cl, Br$) in the gas phase optimized at the DFT/PBE0 level of theory.

of the ground-state molecular geometries were optimized including the relativistic effects at the spin-free level in the gas phase and with solvent effects using density functional theory (DFT). The Kohn-Sham equation was solved using the hybrid PBE0 functional [27]. The structure of the first low-lying excited state was optimized using the time-dependent (TD)-DFT/PBE0 method as implemented in the Turbomole V7.3 2018 [28] and Gaussian 16 [29] codes. The vibrational harmonic frequencies were computed using either an analytic Hessian matrix or numerical finite differences of the gradient. All geometries considered for the vibronic spectra calculations represent true minima as they have no imaginary frequencies. The optimized structures are available in the Supporting Information.

In these calculations, def2-TZVP (second generation of triple- ζ polarization quality) Karlsruhe basis sets [30, 31] have been used for all light elements (H, C, N, O, Cl). For the heaviest atoms, small-core relativistic effective core pseudopotentials (RECP) were used: namely, the 60-core-electron RECP for uranium [32, 33] along with the def-TZVP (first generation of triple- ζ polarization quality) basis set [34], and the 28-core electrons RECP for bromine with the associated aug-cc-pVTZ-PP basis set [35]. To speed up the calculations, the resolution of the identity approximation to compute the Coulomb integrals (RI-J) [36, 37] with appropriate auxiliary basis sets [34, 38] was employed.

c. Vertical Absorption and Emission Energies. On the basis of the benchmark calculations carried out by Tecmer et al. [9, 39, 40] on a series of uranium(VI)-based

compounds, the CAM-B3LYP [41] exchange-correlation functional was found to be more accurate than the PBE0 functional for uranyl valence transition energies. Thus, to accurately position the “hot bands”, the vertical excitation and emission energies with and without accounting for solvent effects were obtained from the ground- and excited-state structures, respectively, with TD-DFT single-point calculations with the latter functional and the Amsterdam Density Functional package (ADF2018.01) [42]. All atoms were described by TZ2P Slater-type basis sets [43] (triple- ζ with two polarization functions quality), without the frozen core approximation. The scalar relativistic (SR) and spin-orbit coupling (SOC) effects were accounted for by the ZORA Hamiltonian [44].

d. Continuum Solvent Models. Long-range solvent effects were modeled by polarized continuum medium models, with two similar flavors: the continuum polarizable conductor model (CPCM) [45, 46] as implemented in the Gaussian 16 program and the conductor-like screening model (COSMO) model [47–49] as implemented in the ADF package. The relative permittivity values (ϵ_r) used for *n*-dodecane and acetone are 2.006 and 20.493, respectively.

III. RESULTS AND DISCUSSIONS

A. Experimental Luminescence Spectra

The time-resolved luminescence spectrum of the uranyl sample in the presence of chloride ions and Aliquate 336 in *n*-dodecane with 1 % of 1-decanol is shown on Figure 2 (black line). It is superimposed with the spectrum (red line) acquired by Görrler-Walrand et al. [11] under similar conditions and in acetone. The spectrum also compares well with those obtained earlier in chloroaluminate [21], tetraalkylammonium [13] and pyrrolidinium [12] ionic liquids. The spectrum of $[A336]_2[UO_2Cl_4]$ in *n*-dodecane in Figure 2 shows an electronic transition (“hot band”) at low energy about $21\,000\text{ cm}^{-1}$ followed by a series of vibronic peaks in the $20\,300\text{ cm}^{-1}$ to $16\,000\text{ cm}^{-1}$ range, which is typical of the $[UO_2Cl_4]^{2-}$ species with a D_{4h} coordination symmetry [50]. A monoexponential decay with a fluorescence lifetime of $0.3\text{ }\mu\text{s}$ was measured for the uranium(VI) sample in a presence of chloride ions, Aliquate[®] 336 and *n*-dodecane. This confirms the formation of a unique complex, which was assumed to be $[A336]_2[UO_2Cl_4]$ with four chloride ions coordinated to uranyl in its equatorial plane, in line with the extracted complex stoichiometry [14].

The decomposition of the $[A336]_2[UO_2Cl_4]$ luminescence spectra has been performed by Reiller et al. [14]. The resolution of the presently used apparatus did not allow good resolution of some of the transitions and revealed only the wide components which cover several vibronic progressions in one peak. Moreover, a difference in the relative intensities is observed at around $20\,295\text{ cm}^{-1}$

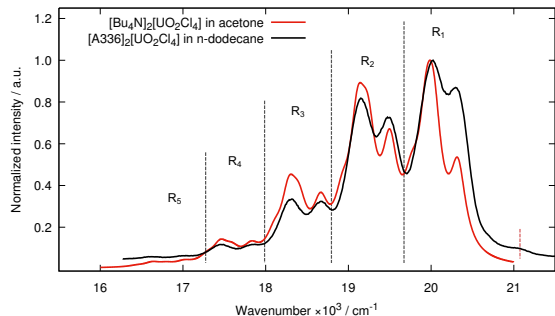


FIG. 2: Recorded time-resolved luminescence spectra of $[\text{Bu}_4\text{N}]_2[\text{UO}_2\text{Cl}_4]$ in acetone (the maxima taken from Görller-Walrand et al. [11] and the Lorentzian shape computed) and $[\text{A336}]_2[\text{UO}_2\text{Cl}_4]$ in *n*-dodecane (this work). The vertical dashed red line shows the “hot band” position and R_n , ($n = 1 - 5$) corresponds to the vibronic progression region. Details on the spectral data are available in Table S1 of the Supporting Information.

in *n*-dodecane due to the long gate width selected to collect more luminescence signals in our measurements. The spectrum in *n*-dodecane is shifted to the blue side by 30 cm^{-1} , in comparison to that in acetone, and only by 5 cm^{-1} with respect to that in $[\text{Bu}_3\text{MeN}][\text{Tf}_2\text{N}]$ ionic liquid [13]. Thus, from the measurements, one can conclude that neither the counterion nor the type of solvent has any significant influence on the position of maxima of the luminescence bands. The change in the relative intensities of the transitions along the vibronic progression has been attributed by Sornein et al. [13] to the formation of $\text{C}-\text{H}\cdots\text{Cl}$ hydrogen bonding between the chloride of the $[\text{UO}_2\text{Cl}_4]^{2-}$ moiety and a hydrogen atom of a cation present in the ionic liquid. As we are using an aprotic solvent (*n*-dodecane), this effect may also be present in our uranyl tetrachloride sample.

The spacing between the vibronic progressions of the luminescence spectrum corresponds to the ground-state uranyl stretching frequency value ν_s . One can extract the ν_s value by only taking into account the spacing between the vibrational maxima of the same nature for $[\text{A336}]_2[\text{UO}_2\text{Cl}_4]$ in *n*-dodecane. The resulting ν_s value amounts to $(836 \pm 18) \text{ cm}^{-1}$, which is in good agreement with the values, 823 ± 14 , 825 , and $(850 \pm 25) \text{ cm}^{-1}$ observed in acetone [11], $[\text{C}_4\text{mim}][\text{Tf}_2\text{N}]$ [12], and in $[\text{Bu}_3\text{MeN}][\text{Tf}_2\text{N}]$ [13], respectively. This vibration corresponds to a Raman-active vibration of the uranyl unit and can be correlated to the $\text{U}-\text{O}_{y1}$ bond length. Using the empiric relation of Bartlett and Cooney [51]

$$R_{\text{U}-\text{O}_{y1}}(\text{\AA}) = 106.5 \times \nu_s^{-2/3} + 0.575 \quad (1)$$

we calculated the $\text{U}-\text{O}_{y1}$ bond length to be equal to $(1.77 \pm 0.01) \text{ \AA}$ (using $\nu_s = (836 \pm 18) \text{ cm}^{-1}$) for our uranyl sample. This value agrees with all experimental data given in Table I and can therefore serve as reference

data to assess the accuracy of the *ab initio* calculations we will now discuss.

B. Ground- and Excited-State Structures of the Uranyl Tetrachloride Complexes

a. Uranyl Tetrachloride Dianions. The structure of the uranyl tetrachloride dianion has been well-studied by the variety of theoretical and experimental techniques [10, 19, 24, 39, 52–55]. The inclusion of all effects to mimic the experimental conditions is challenging for *ab initio* calculations mainly because of the difficulties in building chemically relevant chemical models and the fast growth of the computational costs as the system size grows. The present quantum chemical study was performed on models with increasing chemical complexity to approach the solution sample.

The spin-free optimized ground-state and first excited-state distances between uranium and the coordinated atoms of the $[\text{UO}_2\text{Cl}_4]^{2-}$ and $[\text{UO}_2\text{Br}_4]^{2-}$ together with experimental data are shown in Table I.

In the $[\text{UO}_2\text{Cl}_4]^{2-}$ gas-phase PBE0 calculations, the ground state $\text{U}-\text{O}_{y1}$ bond length of 1.758 \AA is in a good agreement with 1.766 \AA obtained with the CCSD(T) wave-function method, while the $\text{U}-\text{Cl}$ bond length of 2.714 \AA is shorter than 2.735 \AA . Moreover, the PBE0 geometries are in good accordance with the all-electron CAM-B3LYP results reported by Tecmer et al. [39]. This gives us confidence in the ability of PBE0 to provide fairly accurate geometries of the uranium(VI)-containing complexes. The inclusion of solvent effects on $[\text{UO}_2\text{Cl}_4]^{2-}$ does not significantly change the $\text{U}-\text{O}_{y1}$ bond distance in comparison to the gas-phase calculations, but it shortens the $\text{U}-\text{Cl}$ bond length as the solvent polarity increases. Keeping in mind that we do not have strictly the same conditions as in the experiment, it is worth examining trends in both theoretical and experimental data. A comparison of the experimental crystal structure of $\text{Cs}_2\text{UO}_2\text{Cl}_4$ [10] with the structure of uranyl tetrachloride dianion in acetonitrile [53] shows that the $\text{U}-\text{O}_{y1}$ bond length is almost the same under both conditions, while $\text{U}-\text{Cl}$ values are found to be longer in solution by about 0.01 \AA .

To quantify the influence of the ligand nature in the first coordination sphere, the chloride ligands were replaced by bromide ligands, which have the same type of bonding with uranium but larger ionic radii. The uranyl ion coordinated by four bromide ligands has been prepared in crystal form [54], while it is hardly stabilized in solution. The experimental structure of the $\text{Cs}_2\text{UO}_2\text{Br}_4$ crystal shows that the $\text{U}-\text{O}_{y1}$ bond distance (1.777 \AA) is almost equal to that found in the chloride homologue $\text{Cs}_2\text{UO}_2\text{Cl}_4$ ($R_{\text{U}-\text{O}_{y1}} = 1.774 \text{ \AA}$), whereas the $\text{U}-\text{Br}$ distance is longer by 0.149 \AA than that of $\text{U}-\text{Cl}$. The gas-phase geometries of $[\text{UO}_2\text{Cl}_4]^{2-}$ and $[\text{UO}_2\text{Br}_4]^{2-}$ follow this trend; the substitution of chloride by bromide ligands leads to an insignificant stabilization of the $\text{U}-\text{O}_{y1}$

bond, and the U–Br bond distance is longer by 0.169 Å than that of U–Cl, as the U–Br bond is weaker than the U–Cl bond.

The lowest triplet excited state in $[\text{UO}_2\text{X}_4]^{2-}$ complexes corresponds to an excitation of an electron out of an orbital that is a mixture of the bonding σ_u orbital of the uranyl unit and the halide valence p orbitals into the nonbonding δ_u uranium orbital. When the transition occurs the U– O_{y1} bond weakens and the excited state potential curve shifts along the symmetric U– O_{y1} mode to greater U– O_{y1} distances and becomes flatter [23]. Looking at the excited-state geometries of the uranyl tetrahalide dianions, one can note a lengthening of the U– O_{y1} bond by 0.031 and 0.028 Å in $[\text{UO}_2\text{Cl}_4]^{2-}$ and $[\text{UO}_2\text{Br}_4]^{2-}$, respectively, since the excitation depopulates the U– O_{y1} bonding orbital. The differences in the U–X, (X = Cl, Br) bonds are small, about 0.010 Å on average. From highly resolved low-temperature two-photon absorption spectra of $\text{Cs}_2\text{UO}_2\text{Cl}_4$, Denning et al. [19, 50] determined that the U– O_{y1} and U–Cl bonds elongate by 0.070 and 0.014 Å, respectively. Inclusion of long-range solvent effects affect the excited state structure in the same way as for the ground state.

The analysis of the vibrational frequencies is very important for the characterization of the theoretical luminescence spectra, as specific vibrations appear in the vibronic progression. Some of the ground-state vibrational frequencies are responsible for the band spacing in the experimental luminescence spectrum, while the atomic displacement between the ground and excited-state geometries is responsible for the intensity ratio. The U–X ($\nu_{\text{U-X}}$) and U– O_{y1} (ν_s) symmetrical stretching modes and O_{y1} –U– O_{y1} bending mode (ν_b) contribute to the luminescence spectral shape to a large extent, and their values for the $[\text{UO}_2\text{Cl}_4]^{2-}$ and $[\text{UO}_2\text{Br}_4]^{2-}$ complexes are given in Table II. The U– O_{y1} asymmetrical stretching mode (ν_a), which is vibronically silent, is also shown to allow discussion of trends. Using the vibrational perturbation theory [56, 57] as implemented in Gaussian 16 [29], we have computed the anharmonic corrections, which turned out to be small: on the order of 5 and 3 cm^{-1} for the ground and excited states, respectively (see Table S2 in the Supporting Information).

For the gas-phase $[\text{UO}_2\text{Cl}_4]^{2-}$ model, the computed $\nu_{\text{U-Cl}}$, ν_b , ν_s and ν_a frequencies are smaller in the excited state than in the ground state by 4, 4, 80, and 115 cm^{-1} , respectively. The PBE0 calculations reproduce with an impressive accuracy the measured red shift of the stretching mode, ν_s , 82 cm^{-1} , in $\text{Cs}_2\text{UO}_2\text{Cl}_4$, and underestimates that for the bending mode, 20 cm^{-1} . The latter discrepancy has negligible impact as the ν_s dominates the vibronic progressions visible in the luminescence spectra.

Turning now to the vibrational frequencies obtained with solvent effects, we observed an opposite behavior of the U–Cl and U– O_{y1} frequencies. With an increase in polarity the $\nu_{\text{U-Cl}}$ stretching frequencies insignificantly increase (4 and 7 cm^{-1}) for the ground and excited states,

respectively, while the uranyl ν_b , ν_s , and ν_a frequencies decrease by 5 cm^{-1} to 25 cm^{-1} in both states. This shift in the ground-state frequencies should be observable in the computed luminescence spectra, namely in the spacing between the vibrationally resolved peaks, while the change in the excited-state frequencies should only affect the vibronic intensities.

The substitution of chlorides by bromides in the uranyl equatorial plane lead to the following changes in the vibrational spectra. In comparison to uranyl tetrachloride, the ν_b value decreased by less than 10 cm^{-1} in both the ground and excited states. The ν_s values increased by 13 and 62 cm^{-1} in the ground and excited states, respectively. Similarly, the ν_a values increased by 14 cm^{-1} for the ground state and 76 cm^{-1} for the first excited state. The U–Br stretching mode is 83 cm^{-1} lower in both the ground and excited states than the U–Cl symmetric stretching vibration. This is in line with the ground-state experimental trends measured for $\text{Cs}_2\text{UO}_2\text{Cl}_4$ and $[\text{C}_7\text{H}_{16}\text{NO}_2][\text{UO}_2\text{Br}_4]$ (91, 2, 6 and 9 cm^{-1} for $\nu_{\text{U-Br}}$, ν_b , ν_s , and ν_a , respectively). These changes indicate that the bromide ligand has a smaller effect on the electronic structure of uranium than does chloride, since the U–Br interaction has less of an effect on the U– O_{y1} bonding. Consistently, the ν_s frequency is larger than that in $[\text{UO}_2\text{Cl}_4]^{2-}$ and is close to the bare uranyl value. For $[\text{UO}_2\text{Br}_4]^{2-}$ the shifts of vibrational frequencies between the ground and excited state are given in Table S10 in the Supporting Information.

b. Organic Cation Uranyl Tetrachloride: [A336]₂[UO₂Cl₄]. The $[\text{UO}_2\text{Cl}_4]^{2-}$ dianion in interaction with the organic ligand has been prepared under the conditions described in the Experimental Section. The final compound is predicted to be the uranyl tetrachloride associated with two extractant cations of methyltrioctylammonium $[\text{A336}]_2[\text{UO}_2\text{Cl}_4]$ as a result of an ion-exchange mechanism [14]. Interestingly, Görller-Warland et al. [11] stabilized the $[\text{UO}_2\text{Cl}_4]^{2-}$ dianion in solution with tetrabutylammonium chloride (Bu_4NCl), a ligand belonging to the same group of tetraalkylammonium salts as Aliquate 336. For our purpose, the geometries of the ground and luminescent states of both complexes were optimized by placing the two countercations in the second coordination sphere in a *trans* position. The bond distances are shown in Table III, while the vibrational frequencies are shown in Table II.

If one compares the computed geometrical parameters to those of the models without an explicit second-coordination sphere (Table I), the countercations induce a weakening of the uranyl bond and loss of the D_{4h} symmetry. These changes are due to the presence of weak hydrogen bonds between the hydrogen atoms of the alkyl chains of the cation with the oxygen and chloride atoms of the uranyl tetrachloride unit [13] (see Figure S3 and Table S3 in the Supporting Information). The ground-state geometries of uranyl tetrachloride in $[\text{Bu}_4\text{N}]_2[\text{UO}_2\text{Cl}_4]$ and $[\text{A336}]_2[\text{UO}_2\text{Cl}_4]$ have been found

TABLE I: Ground- and Excited State Geometries of $[\text{UO}_2\text{X}_4]^{2-}$ ($\text{X} = \text{Cl}, \text{Br}$) Compared to Selected Previous Results

	$\text{R}_{\text{U}-\text{O}_{\text{y1}}}, \text{\AA}$	$\text{R}_{\text{U}-\text{X}}, \text{\AA}$	Compound/media	Method	Ref.
Ground state					
$[\text{UO}_2\text{Cl}_4]^{2-}$	1.758	2.714	gas-phase	R-ECP/PBE0	this work
	1.766	2.735	gas-phase	CCSD(T)	[52]
	1.764	2.712	gas-phase	all-electron/CAM-B3LYP	[39]
	1.774	2.671	$\text{Cs}_2\text{UO}_2\text{Cl}_4$	X-ray	[10]
	1.759	2.699	CPCM n-dodecane	R-ECP/PBE0	this work
	1.761	2.683	CPCM acetone	R-ECP/PBE0	this work
	1.770	2.680	acetonitrile	EXAFS	[53]
$[\text{UO}_2\text{Br}_4]^{2-}$	1.750	2.883	gas-phase	R-ECP/PBE0	this work
	1.749	2.905	gas-phase	R-ECP/CAM-B3LYP	this work
	1.777	2.820	$\text{Cs}_2\text{UO}_2\text{Br}_4$	X-ray	[54]
Excited state					
$[\text{UO}_2\text{Cl}_4]^{2-}$	1.789	2.721	gas-phase	R-ECP/PBE0	this work
	1.844	2.685	$\text{Cs}_2\text{UO}_2\text{Cl}_4$	Two-photon absorption	[19]
	1.790	2.706	CPCM n-dodecane	R-ECP/PBE0	this work
	1.791	2.692	CPCM acetone	R-ECP/PBE0	this work
$[\text{UO}_2\text{Br}_4]^{2-}$	1.778	2.895	gas-phase	R-ECP/PBE0	this work
	1.780	2.918	gas-phase	R-ECP/CAM-B3LYP	this work

TABLE II: Ground- and Excited-State Vibrational Frequencies (in cm^{-1}) of the $[\text{R}_4\text{N}]_2[\text{UO}_2\text{X}_4]$, ($[\text{R}_4\text{N}] = [\text{Bu}_4\text{N}], [\text{A336}]$) Compounds

System	$\nu_{\text{U}-\text{X}}$	ν_{b}	ν_{s}	ν_{a}	Method	Ref.
Ground state						
$[\text{UO}_2\text{Cl}_4]^{2-}$	237	275	894	974	R-ECP/PBE0 gas-phase	this work
	235	269	889	960	R-ECP/PBE0 n-dodecane	this work
	241	265	889	949	R-ECP/PBE0 acetone	this work
	264 [19]	250	832	915	Raman and IR in solid	[50]
$\text{Cs}_2\text{UO}_2\text{Cl}_4$						
$[\text{Me}_4\text{N}]_2[\text{UO}_2\text{Cl}_4]$			831	909	Raman and IR in solid	[58]
$[\text{Et}_4\text{N}]_2[\text{UO}_2\text{Cl}_4]$	240	263	869		Raman in solid	[59]
$[\text{Bu}_4\text{N}]_2[\text{UO}_2\text{Cl}_4]$	270	286	869	945	R-ECP/PBE0 gas-phase	this work
	258	262	833	919	Raman and IR in CH_2Cl_2 solution	[60]
$[\text{A336}]_2[\text{UO}_2\text{Cl}_4]$	266	288	876	957	R-ECP/PBE0 gas-phase	this work
$[\text{UO}_2\text{Br}_4]^{2-}$	144	262	907	988	R-ECP/PBE0 gas-phase	this work
	173	252	826	904	Raman and IR in solid	[61]
Excited state						
$[\text{UO}_2\text{Cl}_4]^{2-}$	233	271	814	859	R-ECP/PBE0 gas-phase	this work
	236	268	811	854	R-ECP/PBE0 n-dodecane	this work
	240	263	808	848	R-ECP/PBE0 acetone	this work
$\text{Cs}_2\text{UO}_2\text{Cl}_4$		230	750	830	N.A.	[11]
$[\text{Bu}_4\text{N}]_2[\text{UO}_2\text{Cl}_4]$	266	281	799	845	R-ECP/PBE0 gas-phase	this work
$[\text{A336}]_2[\text{UO}_2\text{Cl}_4]$	261	284	802	854	R-ECP/PBE0 gas-phase	this work
$[\text{UO}_2\text{Br}_4]^{2-}$	151	264	876	935	R-ECP/PBE0 gas-phase	this work

to be nearly the same; the $\text{U}-\text{O}_{\text{y1}}$ bond lengths are longer by about 0.010\AA than in the bare $[\text{UO}_2\text{Cl}_4]^{2-}$ complex. Moreover, because of the symmetry distortion and interaction of chloride ligands with the counterion, the $\text{U}-\text{Cl}$ distances differ by 0.026 up to 0.118\AA in comparison to the bare $[\text{UO}_2\text{Cl}_4]^{2-}$. Even though our theoretical model

does not account for the long-range effects induced by the presence of other species beyond the second coordination sphere, these gas-phase structures are in good accordance with the experimental crystal structures measured for parent compounds with a shorter alkyl chain, such as $[\text{Me}_4\text{N}]_2[\text{UO}_2\text{Cl}_4]$ and $[\text{Et}_4\text{N}]_2[\text{UO}_2\text{Cl}_4]$ [58]. This observation makes us conclude that the chain length of

a tetraalkylammonium cation has no influence on the U–O_{yl} and U–Cl bond-length values and that both organic counteranions (R₄N) interact with the uranyl tetrachloride dianion in a similar way. Since the influence of long-range solvent effects on the bare [UO₂Cl₄]²⁻ complexes is negligible, we rely in the following on the gas-phase structures for the [R₄N]₂[UO₂Cl₄] complexes.

The addition of two counteranions in our chemical model does not change the nature of the first excited state. As a result, the luminescent-state geometry is not significantly affected by the counteranions: in comparison to the bare [UO₂Cl₄]²⁻ complexes, the U–O_{yl} bond length stretches by 0.028 Å for [R₄N]₂[UO₂Cl₄] and the U–Cl distances are from 0.003 to 0.027 Å longer for both types of complexes.

The calculated frequencies have been compared with data from experimental Raman and IR measurements of different crystals or liquid samples of [R₄N]₂[UO₂Cl₄] [58–60]. The computed symmetrical stretching frequency ν_s for [Bu₄N]₂[UO₂Cl₄] matches the value measured for the [Et₄N]₂[UO₂Cl₄] crystal [59]. For [Bu₄N]₂[UO₂Cl₄], the gas-phase computed frequencies ν_{U-Cl} , ν_b , ν_s and ν_a are overestimated by 12, 24, 36 and 26 cm⁻¹, respectively, with respect to the values measured in dichloromethane solution [60]. From emission spectroscopy measurements the symmetrical stretching vibrational frequencies (ν_s) for [Bu₄N]₂[UO₂Cl₄] in acetone and for [A336]₂[UO₂Cl₄] in *n*-dodecane were estimated as 823 [11] and 836 cm⁻¹, respectively. Our gas-phase calculations for these exact complexes yield slightly blue-shifted values: 869 and 876 cm⁻¹.

The differences in computed harmonic frequencies of [UO₂Cl₄]²⁻ in the two [R₄N]₂[UO₂Cl₄] complexes are found to be small. The counterions in the second coordination sphere only slightly affect the calculated frequencies with respect to the bare [UO₂Cl₄]²⁻ ion; the ν_{U-Cl} value is 29 cm⁻¹ higher and the ν_b value has increased by 13 cm⁻¹, while the ν_s and ν_a modes were found to be lower by 18 and 14 cm⁻¹, respectively. This is a result of the loss of symmetry together with the interplay of some motions of hydrogen and carbon atoms in alkyl chain in the vibrational motions. On the basis of the Franck-Condon principle, one can note that it should improve the band spacing between the vibronic progressions of theoretical luminescence spectrum that will be discussed below.

The shifts of theoretical frequencies between the ground and excited states of [A336]₂[UO₂Cl₄] are found to be similar to what was experimentally obtained for Cs₂UO₂Cl₄. The computed uranyl symmetrical stretching mode shifted by 74 cm⁻¹, very close to the experimental value of 82 cm⁻¹. However, the ν_{U-Cl} and ν_b values do not vary during the excitation.

C. Theoretical Absorption and Emission Energies

As the luminescence spectrum of uranium (VI) complexes arises from the electronic transition from the lowest excited state to the ground state, coupled with the progression of vibronic bands, the examination of the whole electronic spectrum is pointless. In this step, we aim at foreseeing the sensitivity to the quantum chemical method of the first triplet excited state absorption and emission energies of the uranyl tetrachloride complex and of the spectral features of uranium (VI) complexes.

The [UO₂Cl₄]²⁻ dianion electronic spectrum has been computed previously with different levels of theory, and detailed discussions of the electronic structure can be found in the literature [23–25, 39]. From previous studies it is known that for a uranyl dication coordinated by ligands the lowest excited state arises from the σ_u highest molecular orbital (HOMO) to the δ_u lowest unoccupied orbital (LUMO). The HOMO corresponds to the bonding combination of uranium 5f and 6p oxygen 2p atomic orbitals and the 3p orbital of first-shell ligands, while the LUMO is a nonbonding uranium 5f orbital (Figure 3). The detailed analysis of the atomic orbitals contributions performed with multireference CASSCF (complete active space self-consistent field) calculations by Pierloot and van Besien [24] suggests that the lowest-lying excitation corresponds to a metal-centered transition from the bonding to nonbonding orbital of uranium, with a marginal ligand-to-metal charge transfer character. Hence, we can use in our discussion the UO₂²⁺ spin-free notation ($D_{\infty h}$), thus labeling the ground state as ¹ Σ_g^+ and the luminescent state as ³ Δ_g .

The vertical absorption (E_{VA}) and emission (E_{VE}) energies were obtained at the all-electron SOC CAM-B3LYP level of theory and are reported here together with experimental values (Table IV). They were computed with the summation of the fully relativistic electronic vertical energies associated with the spin-free zero-point energy correction. It should be noted that the experimental data correspond to the band-origin values obtained from polarized absorption or luminescence spectra and emission energies taken from UV-visible spectroscopic measurements. Thus, a direct comparison with theoretical results is not relevant, but rather we discuss whether the theoretical data reproduce the experimental trends.

As seen in Table IV, the vertical absorption energy of [UO₂Cl₄]²⁻ increases by 85 cm⁻¹ with the addition of acetone due to its small polarity. A blue shift of 117 cm⁻¹ is observed when chlorides are replaced by bromide ligands. In contrast, the band origins seem red-shifted by 128 cm⁻¹ from chloride to bromide complexes according to experimental data [50, 62]. The presence of multiple nonequivalent uranyl sites in the [UO₂Br₄]²⁻ crystal studied by Flint et al. [62] may cause a reverse shift of the whole spectrum and hamper a direct comparison between theoretical and experimental results.

The luminescent state is known to be more sensitive

TABLE III: Ground- and Excited-State Geometries of the $[\text{R}_4\text{N}]_2[\text{UO}_2\text{Cl}_4]$ Compounds Compared to Selected Experimental Results

	$R_{\text{U}-\text{O}_{\text{v}1}}, \text{Å}$	$R_{\text{U}-\text{Cl}}, \text{Å}$	Compound	Method	Ref.
Ground state					
	1.766(6)	2.648(1)-2.677(1)	$[\text{Me}_4\text{N}]_2[\text{UO}_2\text{Cl}_4]$	X-ray	[58]
	1.76(2)-1.77(3)	2.65(1)-2.68(1)	$[\text{Et}_4\text{N}]_2[\text{UO}_2\text{Cl}_4]$	X-ray	[58]
	1.769	2.596-2.753	$[\text{Bu}_4\text{N}]_2[\text{UO}_2\text{Cl}_4]$	R-ECP/PBE0	this work
	1.767	2.609-2.740	$[\text{A336}]_2[\text{UO}_2\text{Cl}_4]$	R-ECP/PBE0	this work
Excited state					
	1.796	2.599-2.780	$[\text{Bu}_4\text{N}]_2[\text{UO}_2\text{Cl}_4]$	R-ECP/PBE0	this work
	1.795	2.614-2.761	$[\text{A336}]_2[\text{UO}_2\text{Cl}_4]$	R-ECP/PBE0	this work

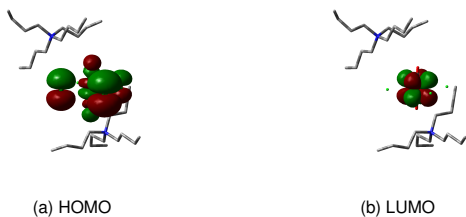
 TABLE IV: Experimental and Computed Vertical Absorption (E_{VA}) and Vertical Emission (E_{VE}) Energies of Uranyl Tetrahalide Complexes (in cm^{-1}). The computed values are obtained at the all-electron SOC CAM-B3LYP level of theory, and corrected with the spin-free Zero-Point Energy correction of the ground and luminescent states

	Theor.		Exp.	
	E_{VA}	E_{VE}	Band-origin	Emission
$[\text{UO}_2\text{Cl}_4]^{2-}$ gas-phase	20737	19924	20096	^a
$[\text{UO}_2\text{Cl}_4]^{2-}$ acetone	20822	20116		
$[\text{UO}_2\text{Br}_4]^{2-}$ gas-phase	20746	20041	19968	^b
$[\text{Bu}_4\text{N}]_2[\text{UO}_2\text{Cl}_4]$ acetone		20009	20097	^c 21000
$[\text{A336}]_2[\text{UO}_2\text{Cl}_4]$ <i>n</i> -dodecane		20041		21025

^a Ref. [50], ^b Ref. [62], ^c Ref. [11]

to the solvent polarity [63]. We indeed observed a larger shift of about 192 cm^{-1} with the inclusion of acetone solvent in comparison to that for absorption energies. With addition of Bu_4N in the second coordination sphere, the E_{VE} increased by 85 cm^{-1} , as expected since the displacements between the ground- and excited-state $[\text{UO}_2\text{Cl}_4]^{2-}$ geometries are larger with than without counter cations. Both theoretical E_{VE} and experimental emission energies of $[\text{UO}_2\text{Cl}_4]^{2-}$ are blue shifted by 32 or 25 cm^{-1} on immersion in *n*-dodecane or acetone, respectively.

It is worth noting that in the experimental spectra, the band-origin values of $[\text{UO}_2\text{Cl}_4]^{2-}$ are the same within 1 cm^{-1} in the $\text{Cs}_2\text{UO}_2\text{Cl}_4$ crystal and in $[\text{Bu}_4\text{N}]_2[\text{UO}_2\text{Cl}_4]$ in acetone. This is fully consistent with the fact that the singly occupied molecular orbitals in the luminescent state do not show any contribution from the second-sphere counterions (See Figure 3).


 FIG. 3: Highest occupied (HOMO) and lowest unoccupied molecular orbitals (LUMO) of $[\text{Bu}_4\text{N}]_2[\text{UO}_2\text{Cl}_4]$ in the gas phase obtained at the RECP DFT/PBE0 level of theory.

D. Theoretical Luminescence Spectra

To simplify the comparison within all spectra, those obtained from our quantum chemical calculations or from experiment, they are all normalized so that the first peak in the low-energy region matches the experimental amplitude. Neither homogeneous nor heterogeneous line broadening effects are included in our computed spectra because of their complicated prediction [2]. We will thus restrict ourselves to discussing the stick spectra.

The most relevant parameters influencing the spectral intensity distribution are the vibrational wave functions of both initial and excited states. The spectral shape is significantly linked to the bond-length changes between the two electronic states, as identified by Su et al. [4] thanks to a semiclassical vibronic approach. In that study, they solely considered the progression of one vibrational mode ν_s . They concluded that the computed bond-length of the excited state is estimated without a sufficient accuracy to properly simulate the intensities. In our study, the theoretical luminescence spectra of $[\text{UO}_2\text{Cl}_4]^{2-}$ and $[\text{UO}_2\text{Br}_4]^{2-}$ in gas phase were obtained by including all vibrational modes to be able to assign all the fine details of the measured vibrational progressions. The theoretical spectra are displayed in Figure 4. The first band appearing in the progression corresponds to the 0-0 vibrational transition. In all uranium(VI) compounds at room temperature (300 K), luminescence arises from a low oscillator strength electronic transition followed by the vibrational progression in the ν_s mode of

the electronic ground state equal to 894 cm^{-1} . Because ν_s is totally symmetrical, it preserves the symmetry of the vibronic (electronic+vibrational) wave function. In $[\text{UO}_2\text{Cl}_4]^{2-}$, the totally symmetrical $\nu_{\text{U-Cl}}$ mode is also excited vibronically, therefore contributing to a line in the vibronic progression which is distant from the 0-0 line by 235 cm^{-1} . However, as we already commented upon the fact that the U–X lengthening from the ground and excited states is underestimated by our quantum approach, we cannot expect the computed relative intensities to match the experimental intensities. Still, our predicted spectra place the peak distribution and band spacing in great agreement with the experimental results. As other vibronic transitions might not be easily visible in Figure 4, we provide a detailed assignment in the Supporting Information.

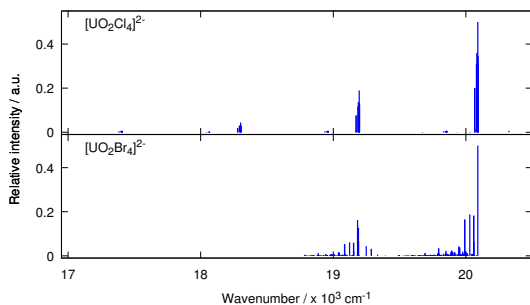


FIG. 4: Theoretical luminescence spectra of $[\text{UO}_2\text{Cl}_4]^{2-}$ and $[\text{UO}_2\text{Br}_4]^{2-}$ in the gas phase computed at 300 K.

Setting the $[\text{UO}_2\text{Cl}_4]^{2-}$ spectra computed in the gas phase side-by-side with those computed in *n*-dodecane and acetone solvents (see Figure S2 in the Supporting Information) reveals that long-range solvent interactions have a minor influence on the spectral profiles, mostly on the intensities of $\nu_{\text{U-X}}$ vibrational mode contributions. Nevertheless, the $[\text{UO}_2\text{Br}_4]^{2-}$ luminescence spectrum displays some more intense contributions and longer vibronic progressions in comparison to $[\text{UO}_2\text{Cl}_4]^{2-}$ (see the bottom panel on Figure 4). This is due to a larger geometrical displacement between the ground- and excited-state structures (see Table S10 in the Supporting Information), which leads to the appearance of U–Br in-plane bending mode progression, distant by 96 cm^{-1} from the 0-0 line.

The computed luminescence spectrum of $[\text{A336}]_2[\text{UO}_2\text{Cl}_4]$ in the gas phase is overlaid with the experimental spectrum in Figure 5. This figure highlights the fact that both the energy positions and the band spacings of the computed vibronic transitions match nicely the experimental envelope, though with the reservation that the band spacing is somewhat red-shifted, as the ground-state symmetrical stretching is slightly overestimated by the R-ECP DFT/PBE0 level of theory and anharmonicity corrections are not accounted for. The vibronic progressions do not change

significantly in comparison to bare $[\text{UO}_2\text{Cl}_4]^{2-}$. In agreement with the results of Görller-Walrand et al. [11], our theoretical approach embeds four vibronic progressions (see Table S8 in the Supporting Information), the first progression being from ν_s , which is in our calculation just 40 cm^{-1} shifted in comparison to experiment, and the second from the rocking vibrational modes. While Görller-Walrand et al. attributed the other progressions to the out-of-plane bending of the chloride anions, our analysis assigns them to the symmetrical and antisymmetrical Cl–U–Cl stretchings.

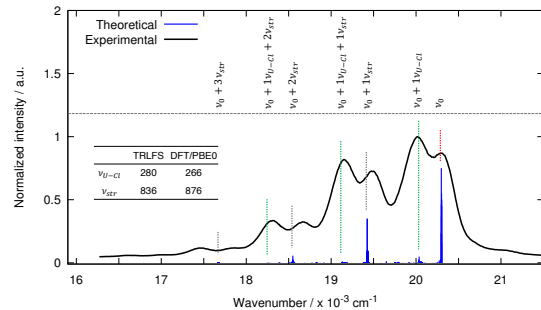


FIG. 5: Experimental and theoretical luminescence spectra of $[\text{A336}]_2[\text{UO}_2\text{Cl}_4]$ in *n*-dodecane and the gas phase, respectively at 300 K.

IV. CONCLUSIONS

Probing and quantifying the long-range effects of large organic counteranions on $[\text{UO}_2\text{Cl}_4]^{2-}$ complex luminescence spectra was realized by two approaches: one experimental using TRFLS and the second using *ab initio*-based approaches. For the latter, relativistic DFT quantum chemical methods were found to be quantitative and effective tools to rationalize and predict uranium(VI)-based complex luminescence properties. Thanks to a benchmark with respect to previous studies on $[\text{UO}_2\text{Cl}_4]^{2-}$ in the crystal and solvent phases, we have been able to assess the degree of reliability of such an approach by a comparison of ground- and luminescent-states structures and frequencies. However, this theoretical protocol reaches some limitations, since we were not able to compute the exact geometrical displacements of the complexes upon excitation from the ground to the first excited state. As a result, the computed intensities of the vibronic bands do not coincide with the experimental intensities. Conversely, the peak positions of the luminescence spectra are correctly reproduced, and the band spacings and theoretical assignments are in good accordance with our experimental data.

In this work, we have used stepwise growth chemical models to quantify the influence of (i) the first coordination sphere by substituting chloride anions by bromides,

(ii) the influence of second-sphere counteractions, and (iii) long-range solvent effects with a polarizable continuum model, with the aim of approaching the experimental conditions. We have found that both long-range solvent effects and the second coordination sphere have little influence on the vibronic intensities, while their effect is more significant for the prediction of other spectroscopic parameters, such as emission energies and vibronic band spacings of the $[\text{UO}_2\text{Cl}_4]^{2-}$ complex. This also confirms that TRIFS spectroscopy may not be sensitive enough to discriminate long-range interactions induced by the counteractions present in the vicinity of the luminescent center.

ACKNOWLEDGEMENTS

We acknowledge support by the French government through the Program "Investissement d'avenir" (LABEX CaPPA / ANR-11-LABX-0005-01 and I-SITE ULNE / ANR-16-IDEX-0004 ULNE), as well as by the Ministry of Higher Education and Research, Hauts de France coun-

cil and European Regional Development Fund (ERDF) through the Contrat de Projets État-Région (CPER CLIMIBIO). Furthermore, this work was granted access to the HPC resources of [CINES/IDRIS/TGCC] under the allocation 2018-2019 [A0050801859] made by GENCI. We also acknowledge the CEA for the Ph.D. grant given to H.O.

ASSOCIATED CONTENT

The following file supplemental-uo2x4-Oher.pdf is available free of charge. It contains:

- Theoretical spectra of the $[\text{UO}_2\text{Cl}_4]^{2-}$ obtained with the long-range counterion and solvent effects.
- Assignments for theoretical and experimental spectra.
- Cartesian coordinates for the calculated structures.

-
- [1] J. Višňák and L. Sobek, *EPJ. Web Conf.* **128**, 02002 (2016).
- [2] J. Su, Y.-L. Wang, F. Wei, W. Schwarz, and J. Li, *J. Chem. Theory Comput.* **7**, 3293 (2011).
- [3] J. Su, Z. Wang, D. Pan, and J. Li, *Inorg. Chem.* **53**, 7340 (2014).
- [4] J. Su, K. Zhang, W. E. Schwarz, and J. Li, *Inorg. Chem.* **50**, 2082 (2011).
- [5] P. Pyykkö, *Chem. Rev.* **88**, 563 (1988).
- [6] K. G. Dyall and K. Fægri, *Introduction to relativistic quantum chemistry* (Oxford University Press, New York, 2007).
- [7] J. Autschbach, *J. Chem. Phys.* **136**, 150902 (2012).
- [8] M. Reiher and A. Wolf, *Relativistic Quantum Chemistry: The Fundamental Theory of Molecular Science, 2nd ed.* (Wiley-VCH, 2014).
- [9] P. Tecmer, A. S. P. Gomes, U. Ekström, and L. Visscher, *Phys. Chem. Chem. Phys.* **13**, 6249 (2011).
- [10] D. J. Watkin, R. G. Denning, and K. Prout, *Acta Crystallogr., Sect. C: Cryst. Struct. Commun.* **47**, 2517 (1991).
- [11] C. Görrler-Walrand, S. De Houwer, L. Fluyt, and K. Binnemans, *Phys. Chem. Chem. Phys.* **6**, 3292 (2004).
- [12] P. Nockemann, K. Servaes, R. Van Deun, K. Van Hecke, L. Van Meervelt, K. Binnemans, and C. Görrler-Walrand, *Inorg. Chem.* **46**, 11335 (2007).
- [13] M.-O. Sornie, C. Cannes, C. Le Naour, G. Lagarde, E. Simoni, and J.-C. Berthet, *Inorg. Chem.* **45**, 10419 (2006).
- [14] P. E. Reiller and C. Mariet, *Radiochim. Acta* (2019), 10.1515/ract-2019-3177.
- [15] G. Hellé, C. Mariet, and G. Cote, *Talanta* **139**, 123 (2015).
- [16] G. Hellé, C. Mariet, and G. Cote, *Microfluid. Nanofluid.* **17**, 1113 (2014).
- [17] T. Vercouter, P. Vitorge, B. Amekraz, and C. Moulin, *Inorg. Chem.* **47**, 2180 (2008).
- [18] V. Mozhayskiy and A. Krylov, "ezspectrum, <http://iopenshell.usc.edu/downloads/>," .
- [19] R. G. Denning, *J. Phys. Chem. A* **111**, 4125 (2007).
- [20] R. G. Denning, C. N. Ironside, J. R. G. Thorne, and D. R. Woodwark, *Mol. Phys.* **44**, 209 (1981).
- [21] T. A. Hopkins, J. M. Berg, D. A. Costa, W. H. Smith, and H. J. Dewey, *Inorg. Chem.* **40**, 1820 (2001).
- [22] F. Ruipérez and U. Wahlgren, *J. Phys. Chem. A* **114**, 3615 (2010).
- [23] K. Pierloot, E. van Besien, E. van Lenthe, and E. J. Baerends, *J. Chem. Phys.* **126**, 194311 (2007).
- [24] K. Pierloot and E. van Besien, *J. Chem. Phys.* **123**, 204309 (2005).
- [25] S. Matsika and R. M. Pitzer, *J. Phys. Chem. A* **105**, 637 (2001).
- [26] A. S. P. Gomes, C. R. Jacob, F. Réal, L. Visscher, and V. Vallet, *Phys. Chem. Chem. Phys.* **15**, 15153 (2013).
- [27] M. Ernzerhof and G. E. Scuseria, *J. Chem. Phys.* **110**, 5029 (1999).
- [28] "TURBOMOLE V7.3 2018, a development of University of Karlsruhe and Forschungszentrum Karlsruhe GmbH, TURBOMOLE GmbH, since 2007; available from <http://www.turbomole.com/>" (1989-2007).
- [29] M. J. Frisch, G. W. Trucks, H. B. Schlegel, G. E. Scuseria, M. A. Robb, J. R. Cheeseman, G. Scalmani, V. Barone, G. A. Petersson, H. Nakatsuji, X. Li, M. Caricato, A. V. Marenich, J. Bloino, B. G. Janesko, R. Gomperts, B. Mennucci, H. P. Hratchian, J. V. Ortiz, A. F. Izmaylov, J. L. Sonnenberg, D. Williams-Young, F. Ding, F. Lipparini, F. Egidi, J. Goings, B. Peng, A. Petrone, T. Henderson, D. Ranasinghe, V. G. Zakrzewski, J. Gao, N. Rega, G. Zheng, W. Liang, M. Hada, M. Ehara, K. Toyota, R. Fukuda, J. Hasegawa, M. Ishida, T. Nakajima, Y. Honda, O. Kitao, H. Nakai,

- T. Vreven, K. Throssell, J. A. Montgomery, Jr., J. E. Peralta, F. Ogliaro, M. J. Bearpark, J. J. Heyd, E. N. Brothers, K. N. Kudin, V. N. Staroverov, T. A. Keith, R. Kobayashi, J. Normand, K. Raghavachari, A. P. Rendell, J. C. Burant, S. S. Iyengar, J. Tomasi, M. Cossi, J. M. Millam, M. Klene, C. Adamo, R. Cammi, J. W. Ochterski, R. L. Martin, K. Morokuma, O. Farkas, J. B. Foresman, and D. J. Fox, "Gaussian-16 Revision B.01," (2016), gaussian Inc. Wallingford CT.
- [30] F. Weigend, M. Häser, H. Patzelt, and R. Ahlrichs, *Chem. Phys. Lett.* **294**, 143 (1998).
- [31] F. Weigend and R. Ahlrichs, *Phys. Chem. Chem. Phys.* **7**, 3297 (2005).
- [32] W. Küchle, M. Dolg, H. Stoll, and H. Preuss, *J. Chem. Phys.* **100**, 7535 (1994).
- [33] X. Cao, M. Dolg, and H. Stoll, *J. Chem. Phys.* **118**, 487 (2003).
- [34] K. Eichkorn, F. Weigend, O. Treutler, and R. Ahlrichs, *Theor. Chem. Acc.* **97**, 119 (1997).
- [35] K. A. Peterson, D. Figgen, E. Goll, H. Stoll, and M. Dolg, *J. Chem. Phys.* **119**, 11113 (2003).
- [36] P. Deglmann, K. May, F. Furche, and R. Ahlrichs, *Chem. Phys. Lett.* **384**, 103 (2004).
- [37] R. Bauernschmitt, M. Häser, O. Treutler, and R. Ahlrichs, *Chem. Phys. Lett.* **264**, 573 (1997).
- [38] F. Weigend, *Phys. Chem. Chem. Phys.* **8**, 1057 (2006).
- [39] P. Tecmer, R. Bast, K. Ruud, and L. Visscher, *J. Phys. Chem. A* **116**, 7397 (2012).
- [40] P. Tecmer, N. Govind, K. Kowalski, W. A. De Jong, and L. Visscher, *J. Chem. Phys.* **139**, 034301 (2013).
- [41] T. Yanai, D. P. Tew, and N. C. Handy, *Chem. Phys. Lett.* **393**, 51 (2004).
- [42] E. J. Baerends, T. Ziegler, A. J. Atkins, J. Autschbach, D. Bashford, O. Baseggio, A. Bérces, F. M. Bickelhaupt, C. Bo, P. M. Boerritger, L. Cavallo, C. Daul, D. P. Chong, D. V. Chulhai, L. Deng, R. M. Dickson, J. M. Dieterich, D. E. Ellis, M. van Faassen, A. Ghysels, A. Giammona, S. J. A. van Gisbergen, A. Goetz, A. W. Götz, S. Gusarov, F. E. Harris, P. van den Hoek, Z. Hu, C. R. Jacob, H. Jacobsen, L. Jensen, L. Joubert, J. W. Kaminski, G. van Kessel, C. König, F. Kootstra, A. Kovalenko, M. Krykunov, E. van Lenthe, D. A. McCormack, A. Michalak, M. Mitoraj, S. M. Morton, J. Neugebauer, V. P. Nicu, L. Noodleman, V. P. Osinga, S. Patchkovskii, M. Pavanello, C. A. Peeples, P. H. T. Philipsen, D. Post, C. C. Pye, H. Ramanantoanina, P. Ramos, W. Ravenek, J. I. Rodríguez, P. Ros, R. Rüger, P. R. T. Schipper, D. Schlüns, H. van Schoot, G. Schreckenbach, J. S. Seldenthuis, M. Seth, J. G. Snijders, M. Solà, S. M., M. Swart, D. Swerhone, G. te Velde, V. Tognetti, P. Ver-nooij, L. Versluis, L. Visscher, O. Visser, F. Wang, T. A. Wesolowski, E. M. van Wezenbeek, G. Wiesenekker, S. K. Wolff, T. K. Woo, and A. L. Yakovlev, "ADF2018, SCM, Theoretical Chemistry, Vrije Universiteit, Amsterdam, The Netherlands, <https://www.scm.com>,".
- [43] E. van Lenthe and E. J. Baerends, *J. Comput. Chem.* **24**, 1142 (2003).
- [44] E. van Lenthe, E.-J. Baerends, and J. G. Snijders, *J. Chem. Phys.* **99**, 4597 (1993).
- [45] V. Barone and M. Cossi, *The Journal of Physical Chemistry A*, *J. Phys. Chem. A* **102**, 1995 (1998).
- [46] M. Cossi, N. Rega, G. Scalmani, and V. Barone, *J. Comput. Chem.* **24**, 669 (2003).
- [47] A. Klamt and G. Schüürmann, *J. Chem. Soc., Perkin Trans. 2* **5**, 799 (1993).
- [48] A. Klamt, *J. Phys. Chem.* **99**, 2224 (1995).
- [49] A. Klamt and V. Jonas, *J. Chem. Phys.* **105**, 9972 (1996).
- [50] R. G. Denning, T. R. Snellgrove, and D. R. Woodwark, *Mol. Phys.* **32**, 419 (1976).
- [51] J. R. Bartlett and R. P. Cooney, *J. Mol. Struct.* **193**, 295 (1989).
- [52] P. Dau, J. Su, H.-T. Liu, D.-L. Huang, J. Li, and L.-S. Wang, *J. Chem. Phys.* **137**, 064315 (2012).
- [53] K. Servaes, C. Hennig, R. Van Deun, and C. Görrler-Walrand, *Inorg. Chem.* **44**, 7705 (2005).
- [54] R. E. Wilson, S. Skanthakumar, C. Cahill, and L. Soderholm, *Inorg. Chem.* **50**, 10748 (2011).
- [55] N. P. Deifel and C. L. Cahill, *C. R. Chim.* **13**, 747 (2010).
- [56] V. Barone, *J. Chem. Phys.* **120**, 3059 (2004).
- [57] V. Barone, *J. Chem. Phys.* **122**, 014108 (2005).
- [58] D. D. Schnaars and R. E. Wilson, *Inorg. Chem.* **52**, 14138 (2013).
- [59] J. Newbery, *Spectrochim. Acta, Part A* **25**, 1699 (1969).
- [60] M. Gal, P. Goggin, and J. Mink, *J. Mol. Struct.* **114**, 459 (1984).
- [61] A. Marzotto, R. Graziani, G. Bombieri, and E. Forsellini, *J. Cryst. Mol. Struct.* **4**, 253 (1974).
- [62] C. D. Flint and P. A. Tanner, *J. Chem. Soc., Faraday Trans. 2* **78**, 103 (1982).
- [63] J. R. Lakowicz, ed., "Solvent and environmental effects," in *Principles of Fluorescence Spectroscopy* (Springer US, Boston, MA, 2006) pp. 205–235.

Supporting information for:

Investigation of the luminescence of $[\text{UO}_2\text{X}_4]^{2-}$ (X=Cl, Br) complexes in organic phase using time-resolved laser-induced fluorescence spectroscopy and quantum chemical simulations

Hanna Oher,^{†,‡} Florent Ral,[‡] Thomas Vercouter,^{*,†} and Valrie Vallet^{*,‡}

[†]*DEN-Service d'Etudes Analytiques et de Ractivit des Surfaces (SEARS), CEA, Universit
Paris-Saclay, F-91191 Gif-sur-Yvette, France*

[‡]*Univ. Lille, CNRS, UMR 8523 - PhLAM - Physique des Lasers Atomes et Molcules,
F-59000 Lille, France*

E-mail: thomas.vercouter@cea.fr; valerie.vallet@univ-lille.fr

Contents

List of Figures

S1	Normalized time-resolved luminescence spectra of $[A336]_2[UO_2Cl_4]$ in <i>n</i> -dodecane measured at different delay time.	S5
S2	Comparison of reference sample(without U) with the sample of $[A336]_2[UO_2Cl_4]$ in <i>n</i> -dodecane measured at different delay time.	S6
S3	Illustrations of hydrogen bondings between the first and second coordination spheres of uranyl in $[R_4N]_2[UO_2Cl_4]$ complexes. Left panel is representing interactions in $[Bu_4N]_2[UO_2Cl_4]$ and right in $[A336]_2[UO_2Cl_4]$	S16
S4	Influence of solvent effects on the theoretical spectrum of $[UO_2Cl_4]^{2-}$ at 0 K (upper panel) and 300 K (lower panel). The spectral shapes were obtained by a Lorentzian convolution; the assignments are provided in Tables S4, S5 and S6 for the $[UO_2Cl_4]^{2-}$ in gas-phase, <i>n</i> -dodecane and acetone, respectively. . .	S17
S5	Effect of a $[A336]^+$ counter ion on the theoretical $[UO_2Cl_4]^{2-}$ spectrum in gas-phase at 300 K. The spectral shapes were obtained by a Lorentzian convolution; the assignments are provided in Tables S4 and S9 for the $[UO_2Cl_4]^{2-}$ and $[A336]_2[UO_2Cl_4]$, respectively.	S17
S6	Comparison of the theoretical spectra of $[Bu_4N]_2[UO_2Cl_4]$ and $[A336]_2[UO_2Cl_4]$ complexes in a gas-phase at 300 K. The spectral shapes were obtained by a Lorentzian convolution; the assignments are provided in Tables S8 and S9 for the $[Bu_4N]_2[UO_2Cl_4]$ and $[A336]_2[UO_2Cl_4]$, respectively.	S18

List of Tables

- S1 Experimental luminescence data of the $[\text{R}_4\text{N}]_2[\text{UO}_2\text{Cl}_4]$ complexes at room temperature. The ν corresponds to the position of the band, the $\Delta\nu$ is a difference between the bands position in a region, the $\Delta\nu_n$ is a difference between the peaks of the same nature located in different regions. All data are in cm^{-1} . The luminescence spectra are shown on Figure 2 in the main text. S7
- S2 Ground and excited state harmonic and anharmonic frequencies (in cm^{-1}) of the $[\text{UO}_2\text{Cl}_4]^{2-}$ complex in a gas phase computed by G16 at R-ECP DFT/PBE0 and TD-DFT/PBE0 level of theory for the ground and first excited states respectively. S8
- S3 The chloride-hydrogen bond lengths (in Å) in $[\text{R}_4\text{N}]_2[\text{UO}_2\text{Cl}_4]$ complexes computed at the R-ECP DFT/PBE0 and TD-DFT/PBE0 levels of theory for the ground and first excited states, respectively. Atom labeling corresponds to the one shown on Figure S3. S9
- S4 Assignment of the $[\text{UO}_2\text{Cl}_4]^{2-}$ (gas-phase) theoretical luminescence spectrum. The energy of the spectrum was adjusted to experimental band-origin value of $[\text{UO}_2\text{Cl}_4]^{2-}$ in acetone. The nature of bands is explained in Table S2. . . . S10
- S5 Assignment of the $[\text{UO}_2\text{Cl}_4]^{2-}$ (dodecane) theoretical luminescence spectrum. The energy of the spectrum was adjusted to experimental band-origin value of $[\text{UO}_2\text{Cl}_4]^{2-}$ in acetone. The nature of bands is explained in Table S2. . . . S11
- S6 Assignment of the $[\text{UO}_2\text{Cl}_4]^{2-}$ (acetone) theoretical luminescence spectrum. The energy of the spectrum was adjusted to experimental band-origin value of $[\text{UO}_2\text{Cl}_4]^{2-}$ in acetone. The nature of bands is explained in Table S2. . . . S12
- S7 Assignment of the $[\text{UO}_2\text{Br}_4]^{2-}$ theoretical luminescence spectrum. The energy of the spectrum was adjusted to experimental band-origin value of $[\text{UO}_2\text{Cl}_4]^{2-}$ in acetone. The bands representation is taken from the $[\text{UO}_2\text{Cl}_4]^{2-}$ frequencies, the nature of bands is explained in Table S2. S13

S8	Assignment of the $[\text{Bu}_4\text{N}]_2[\text{UO}_2\text{Cl}_4]$ (gas-phase) theoretical luminescence spectrum. The energy of the spectrum was adjusted to experimental band-origin value of $[\text{UO}_2\text{Cl}_4]^{2-}$ in acetone. The nature of bands is shown in Table S2.	S14
S9	Assignment of the $[\text{A336}]_2[\text{UO}_2\text{Cl}_4]$ gas-phase theoretical luminescence spectrum. The energy of the spectrum was adjusted to experimental band-origin value of $[\text{A336}]_2[\text{UO}_2\text{Cl}_4]$ in <i>n</i> -dodecane. The bands representation is taken from the $[\text{UO}_2\text{Cl}_4]^{2-}$ frequencies, with details found in Table S2.	S15
S10	Theoretical displacements of geometries ΔR , and absolute frequency shifts $\Delta\nu$ from the ground to the first excited state.	S15
S11	Cartesian coordinates (in Å) of the $[\text{UO}_2\text{X}_4]^{2-}$ complexes in different media at their ground and first excited state minima obtained by R-ECP DFT/PBE0 and TD-DFT/PBE0 methods, respectively.	S19
S12	Cartesian coordinates (in Å) of the $[\text{Bu}_4\text{N}]_2[\text{UO}_2\text{Cl}_4]$ in gas phase at its ground and first excited state minima obtained in Turbomole 7.3.1 by R-ECP DFT/PBE0 and TD-DFT/PBE0 methods respectively.	S20
S13	Cartesian coordinates (in Å) of the $[\text{A336}]_2[\text{UO}_2\text{Cl}_4]$ in gas phase at its ground and first excited state minima obtained in Turbomole 7.3.1. by R-ECP DFT/PBE0 and TD-DFT/PBE0 methods respectively.	S24

Selection of the delay time

To select a correct delay time for recording of time-resolved spectrum of $[A336]_2[UO_2Cl_4]$ in *n*-dodecane, we have performed measurements at several delay time, 20, 50, 100 and 200 ns. The corresponding recorded spectra are shown in Figure S1.

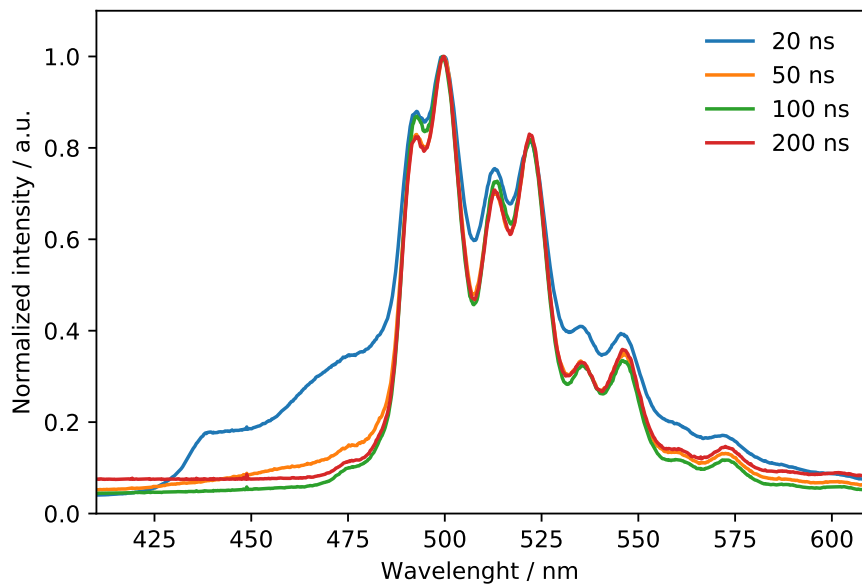
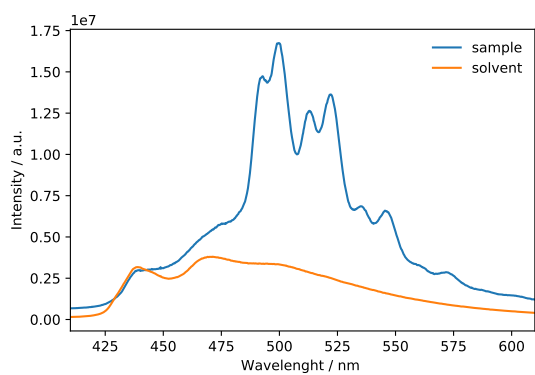


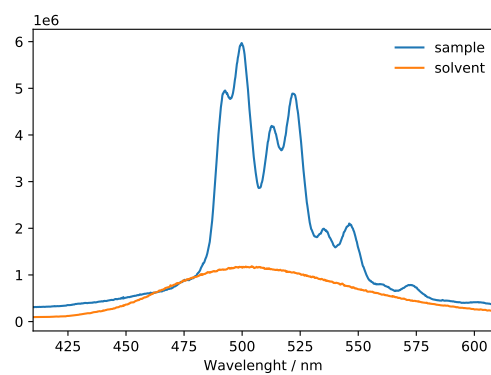
Figure S1: Normalized time-resolved luminescence spectra of $[A336]_2[UO_2Cl_4]$ in *n*-dodecane measured at different delay time.

By inspecting the normalized spectra at different delay times, we have found that positions of maxima remain the same, along with the vibronic features. However, at short delay times (20 and 50 ns), a background luminescence contribution appears in the short wavelength range (around 430 nm), which, by comparison to the spectra of the reference media (solution without uranium), might be attributed to the luminescence of the solvent or the A336 molecule (Figure S2), with its own exponential decay.

This background emission vanished for larger delay times (100, up to 200 ns), and as the recorded spectra are essentially the same for these two-time values, we chose the 100 ns delay time.



(a) 20 ns



(b) 50 ns

Figure S2: Comparison of reference sample(without U) with the sample of $[A336]_2[UO_2Cl_4]$ in *n*-dodecane measured at different delay time.

Supplemental Tables

Table S1: Experimental luminescence data of the $[\text{R}_4\text{N}]_2[\text{UO}_2\text{Cl}_4]$ complexes at room temperature. The ν corresponds to the position of the band, the $\Delta\nu$ is a difference between the bands position in a region, the $\Delta\nu_n$ is a difference between the peaks of the same nature located in different regions. All data are in cm^{-1} . The luminescence spectra are shown on Figure 2 in the main text.

		$[\text{A336}]_2[\text{UO}_2\text{Cl}_4]$ in <i>n</i> -dodecane				$[\text{Bu}_4\text{N}]_2[\text{UO}_2\text{Cl}_4]$ in acetone			
		ν/cm^{-1}	$\Delta\nu$	$\Delta\nu_n$	Intensity	ν/cm^{-1}	$\Delta\nu$	$\Delta\nu_n$	Intensity
Region		21025			0.06				
1	I_1	20295	730		0.84	20325	-		0.74
	I'_1	20015	280		1.00	20032	293		0.95
	I_1^*					19944	88		0.91
						19763	181		0.40
2	I_2	19488	527	807	0.70	19501	262	824	0.84
	I'_2	19155	333	860	0.81	19238	263	794	0.83
	I_2^*					19113	125	831	1.00
						18925	188	838	0.34
3	I_3	18651	504	837	0.28	18664	261	837	0.39
	I'_3	18305	346	850	0.30	18403	261	836	0.36
	I_3^*					18282	121	832	0.51
						18103	179	822	0.16
4	I_4	17839	466	812	0.08	17825	278	838	0.11
	I'_4	17454	385	851	0.08	17593	232	810	0.09
	I_4^*					17452	141	830	0.16
						17289	163	814	0.05
5	I_5	16996	458	843	0.02	17013	277	813	0.03
	I'_5	16625	371	829	0.02	16795	217	798	0.02
	I_5^*					16628	168	824	0.03
						16442	186	847	0.01

Table S2: Ground and excited state harmonic and anharmonic frequencies (in cm^{-1}) of the $[\text{UO}_2\text{Cl}_4]^{2-}$ complex in a gas phase computed by G16 at R-ECP DFT/PBE0 and TD-DFT/PBE0 level of theory for the ground and first excited states respectively.

ν	Ground state		Excited state		Nature of the band
	E_{harm}	E_{anharm}	E_{harm}	E_{anharm}	
1	75.7	76.4	71.3	72.4	out-of-plane asymmetrical Cl-U-Cl bending
2	76.6	76.6	77.2	77.2	in plane Cl-U-Cl bending
3	76.6	76.6	77.2	77.2	
4	97.3	98.0	98.7	99.8	U-Cl scissoring
5	110.0	110.3	104.1	105.0	out-of-plane symmetrical Cl-U-Cl bending
6	197.2	193.7	170.5	166.7	$\text{O}_{y1}-\text{U}-\text{O}_{y1}$ rocking
7	197.2	193.7	170.5	166.7	
8	202.3	202.5	199.2	199.0	asymmetrical Cl-U-Cl stretching
9	219.1	219.2	214.5	214.6	asymmetrical Cl-U-Cl stretching
10	219.1	219.2	214.5	214.6	
11	237.3	237.0	232.6	231.6	symmetrical Cl-U-Cl stretching
12	274.5	271.4	271.8	268.5	$\text{O}_{y1}-\text{U}-\text{O}_{y1}$ bending
13	274.5	271.4	271.8	268.5	
14	894.5	889.4	813.7	810.9	symmetrical $\text{O}_{y1}-\text{U}-\text{O}_{y1}$ stretching
15	974.2	966.9	858.9	854.3	asymmetrical $\text{O}_{y1}-\text{U}-\text{O}_{y1}$ stretching

Table S3: The chloride-hydrogen bond lengths (in Å) in $[\text{R}_4\text{N}]_2[\text{UO}_2\text{Cl}_4]$ complexes computed at the R-ECP DFT/PBE0 and TD-DFT/PBE0 levels of theory for the ground and first excited states, respectively. Atom labeling corresponds to the one shown on Figure S3.

$[\text{Bu}_4\text{N}]_2[\text{UO}_2\text{Cl}_4]$			$[\text{A336}]_2[\text{UO}_2\text{Cl}_4]$		
	GS	ES		GS	ES
Cl33-H83	2.534	2.524	Cl25-H57	2.427	2.411
Cl36-H53	2.642	2.606	Cl28-H48	2.557	2.535
Cl33-H97	2.646	2.632	Cl28-H37	2.656	2.626
Cl36-H71	2.789	2.744	Cl28-H151	2.672	2.685
Cl36-H66	2.893	2.885	Cl27-H71	2.851	2.901

Table S4: Assignment of the $[\text{UO}_2\text{Cl}_4]^{2-}$ (gas-phase) theoretical luminescence spectrum. The energy of the spectrum was adjusted to experimental band-origin value of $[\text{UO}_2\text{Cl}_4]^{2-}$ in acetone. The nature of bands is explained in Table S2.

Region	E, cm^{-1}	$\Delta\nu$, cm^{-1}	I, a.u.	Identification
0	20325.0	—	6.50E-01	$0(0)\rightarrow 1(0)$
	20087.9	237.1	1.43E-02	$0(0)\rightarrow 1(1\nu_{11})$
	19930.6	394.4	1.72E-03	$0(0)\rightarrow 1(2\nu_7)$
	19850.8	474.2	3.29E-04	$0(0)\rightarrow 1(2\nu_{11})$
1	19430.6	894.4	2.46E-01	$0(0)\rightarrow 1(1\nu_{14})$
	19193.5	237.1	7.21E-03	$0(0)\rightarrow 1(1\nu_{11}, 1\nu_{14})$
	19036.2	394.4	6.52E-04	$0(0)\rightarrow 1(2\nu_7, 1\nu_{14})$
	18955.6	475.0	1.84E-04	$0(0)\rightarrow 1(2\nu_{11}, 1\nu_{14})$
2	18536.2	894.4	5.91E-02	$0(0)\rightarrow 1(2\nu_{14})$
	18299.1	237.1	2.11E-03	$0(0)\rightarrow 1(1\nu_{11}, 2\nu_{14})$
	18141.8	394.4	1.56E-04	$0(0)\rightarrow 1(2\nu_7, 2\nu_{14})$
	18061.2	475.0	5.94E-05	$0(0)\rightarrow 1(2\nu_{11}, 2\nu_{14})$
3	17641.8	894.4	1.11E-02	$0(0)\rightarrow 1(3\nu_{14})$
	17404.7	237.1	4.66E-04	$0(0)\rightarrow 1(1\nu_{11}, 3\nu_{14})$
	17247.4	394.4	2.95E-05	$0(0)\rightarrow 1(2\nu_7, 3\nu_{14})$
	17166.7	475.0	1.44E-05	$0(0)\rightarrow 1(2\nu_{11}, 3\nu_{14})$
4	16747.4	894.4	1.80E-03	$0(0)\rightarrow 1(4\nu_{14})$
	16510.3	237.1	8.61E-05	$0(0)\rightarrow 1(1\nu_{11}, 4\nu_{14})$
5	15853.0	894.4	2.62E-04	$0(0)\rightarrow 1(5\nu_{14})$

Table S5: Assignment of the $[\text{UO}_2\text{Cl}_4]^{2-}$ (dodecane) theoretical luminescence spectrum. The energy of the spectrum was adjusted to experimental band-origin value of $[\text{UO}_2\text{Cl}_4]^{2-}$ in acetone. The nature of bands is explained in Table S2.

Region	E, cm^{-1}	$\Delta\nu$, cm^{-1}	I, a.u.	Identification
0	20325.0		6.59E-01	$0(0)\text{->}1(0)$
	20116.9	208.1	1.48E-04	$0(0)\text{->}1(2\nu_5)$
	20085.5	239.5	2.42E-02	$0(0)\text{->}1(1\nu_{11})$
	19926.6	398.4	1.79E-03	$0(0)\text{->}1(2\nu_7)$
	19845.9	479.1	6.63E-04	$0(0)\text{->}1(2\nu_{11})$
1	19435.4	889.6	2.34E-01	$0(0)\text{->}1(1\nu_{14})$
	19227.4	208.1	5.26E-05	$0(0)\text{->}1(2\nu_5, 1\nu_{14})$
	19195.9	239.5	8.19E-03	$0(0)\text{->}1(1\nu_{11}, 1\nu_{14})$
	19037.0	398.4	6.34E-04	$0(0)\text{->}1(2\nu_7, 1\nu_{14})$
	18956.4	479.1	2.17E-04	$0(0)\text{->}1(2\nu_{11}, 1\nu_{14})$
2	18545.9	889.6	5.30E-02	$0(0)\text{->}1(2\nu_{14})$
	18337.8	208.1	1.19E-05	$0(0)\text{->}1(2\nu_5, 2\nu_{14})$
	18306.3	239.5	1.79E-03	$0(0)\text{->}1(1\nu_{11}, 2\nu_{14})$
	18147.5	398.4	1.44E-04	$0(0)\text{->}1(2\nu_7, 2\nu_{14})$
	18066.8	479.1	4.62E-05	$0(0)\text{->}1(2\nu_{11}, 2\nu_{14})$
3	17656.3	889.6	9.47E-03	$0(0)\text{->}1(3\nu_{14})$
	17416.8	239.5	3.09E-04	$0(0)\text{->}1(1\nu_{11}, 3\nu_{14})$
	17257.9	398.4	2.57E-05	$0(0)\text{->}1(2\nu_7, 3\nu_{14})$
4	16766.7	889.6	1.46E-03	$0(0)\text{->}1(4\nu_{14})$
	16527.2	239.5	4.60E-05	$0(0)\text{->}1(1\nu_{11}, 4\nu_{14})$
5	15877.2	889.6	2.01E-04	$0(0)\text{->}1(5\nu_{14})$

Table S6: Assignment of the $[\text{UO}_2\text{Cl}_4]^{2-}$ (acetone) theoretical luminescence spectrum. The energy of the spectrum was adjusted to experimental band-origin value of $[\text{UO}_2\text{Cl}_4]^{2-}$ in acetone. The nature of bands is explained in Table S2.

Region	E, cm^{-1}	$\Delta\nu$, cm^{-1}	I, a.u.	Identification
0	20325.0		5.30E-01	0(0)->1(0)
	20081.4	243.6	1.45E-01	0(0)->1($1\nu_{11}$)
	19929.0	396.0	1.56E-03	0(0)->1($2\nu_7$)
	19838.7	486.3	2.08E-02	0(0)->1($2\nu_{11}$)
	19595.1	729.9	2.10E-03	0(0)->1($3\nu_{11}$)
1	19441.9	883.1	1.79E-01	0(0)->1($1\nu_{14}$)
	19198.3	243.6	4.82E-02	0(0)->1($1\nu_{11}$, $1\nu_{14}$)
	19045.9	396.0	5.28E-04	0(0)->1($2\nu_7$, $1\nu_{14}$)
	18955.6	486.3	6.82E-03	0(0)->1($2\nu_{11}$, $1\nu_{14}$)
2	18558.8	883.1	3.89E-02	0(0)->1($1\nu_{14}$)
	18316.0	242.8	1.03E-02	0(0)->1($1\nu_{11}$, $2\nu_{14}$)
	18162.8	396.0	1.14E-04	0(0)->1($2\nu_7$, $2\nu_{14}$)
	18072.4	486.3	1.44E-03	0(0)->1($2\nu_{11}$, $2\nu_{14}$)
3	17675.6	883.1	6.66E-03	0(0)->1($3\nu_{14}$)
	17432.9	242.8	1.74E-03	0(0)->1($1\nu_{11}$, $3\nu_{14}$)
	17280.5	395.2	1.96E-05	0(0)->1($2\nu_7$, $3\nu_{14}$)
	17189.3	486.3	2.40E-04	0(0)->1($2\nu_{11}$, $3\nu_{14}$)
4	16793.3	882.3	9.80E-04	0(0)->1($4\nu_{14}$)
	16549.8	243.6	2.54E-04	0(0)->1($1\nu_{11}$, $4\nu_{14}$)
5	15910.2	883.1	1.30E-04	0(0)->1($5\nu_{14}$)

Table S7: Assignment of the $[\text{UO}_2\text{Br}_4]^{2-}$ theoretical luminescence spectrum. The energy of the spectrum was adjusted to experimental band-origin value of $[\text{UO}_2\text{Cl}_4]^{2-}$ in acetone. The bands representation is taken from the $[\text{UO}_2\text{Cl}_4]^{2-}$ frequencies, the nature of bands is explained in Table S2.

Region	E, cm^{-1}	$\Delta\nu$, cm^{-1}	I, a.u.	Identification
0	20325.0		4.70E-01	0(0)->1(0)
	20229.0	96.0	1.63E-02	0(0)->1(2 ν_3)
	20181.4	143.6	4.06E-02	0(0)->1(1 ν_{11})
	20081.4	243.6	7.03E-03	0(0)->1(2 ν_8)
	19971.8	353.2	2.07E-03	0(0)->1(2 ν_7)
1	19418.5	906.5	1.53E-01	0(0)->1(1 ν_{14})
	19274.1	144.4	1.54E-02	0(0)->1(1 ν_{11} , 1 ν_{14})
	19174.9	243.6	2.29E-03	0(0)->1(2 ν_8 , 1 ν_{14})
2	18511.2	907.3	2.76E-02	0(0)->1(2 ν_{14})
	18367.6	143.6	3.16E-03	0(0)->1(1 ν_{11} , 2 ν_{14})
	18268.4	242.8	4.13E-04	0(0)->1(2 ν_8 , 2 ν_{14})
3	17604.7	906.5	3.63E-03	0(0)->1(3 ν_{14})
	17461.1	143.6	4.66E-04	0(0)->1(1 ν_{11} , 3 ν_{14})
4	16697.4	907.3	3.88E-04	0(0)->1(4 ν_{14})
	16553.8	143.6	5.49E-05	0(0)->1(1 ν_{11} , 4 ν_{14})
5	15790.9	906.5	3.56E-05	0(0)->1(5 ν_{14})

Table S8: Assignment of the $[\text{Bu}_4\text{N}]_2[\text{UO}_2\text{Cl}_4]$ (gas-phase) theoretical luminescence spectrum. The energy of the spectrum was adjusted to experimental band-origin value of $[\text{UO}_2\text{Cl}_4]^{2-}$ in acetone. The nature of bands is shown in Table S2.

Region	E, cm^{-1}	$\Delta\nu$, cm^{-1}	I, a.u.	Identification
0	20325		1.73E-01	$0(0)\rightarrow 1(0)$
	20114	211	1.24E-04	$0(0)\rightarrow 1(1\nu_7)$
	20092	233	2.29E-03	$0(0)\rightarrow 1(1\nu_8)$
	20056	269	1.32E-03	$0(0)\rightarrow 1(1\nu_{11})$
	19902	423	4.00E-04	$0(0)\rightarrow 1(2\nu_7)$
1	19456	869	5.26E-02	$0(0)\rightarrow 1(1\nu_{14})$
	19245	211	1.47E-05	$0(0)\rightarrow 1(1\nu_7, 1\nu_{14})$
	19223	233	7.05E-04	$0(0)\rightarrow 1(1\nu_8, 1\nu_{14})$
	19187	269	3.53E-04	$0(0)\rightarrow 1(1\nu_{11}, 1\nu_{14})$
	19034	423	1.19E-04	$0(0)\rightarrow 1(2\nu_7, 1\nu_{14})$
2	18588	869	1.03E-02	$0(0)\rightarrow 1(2\nu_{14})$
	18356	232	1.40E-04	$0(0)\rightarrow 1(1\nu_8, 2\nu_{14})$
	18318	269	6.24E-05	$0(0)\rightarrow 1(1\nu_{11}, 2\nu_{14})$
	18165	423	2.32E-05	$0(0)\rightarrow 1(2\nu_7, 2\nu_{14})$
3	17719	869	1.60E-03	$0(0)\rightarrow 1(3\nu_{14})$
	17487	232	2.19E-05	$0(0)\rightarrow 1(1\nu_8, 3\nu_{14})$
4	16851	869	2.14E-04	$0(0)\rightarrow 1(4\nu_{14})$
5	15982	869	2.57E-05	$0(0)\rightarrow 1(5\nu_{14})$

Table S9: Assignment of the $[A336]_2[UO_2Cl_4]$ gas-phase theoretical luminescence spectrum. The energy of the spectrum was adjusted to experimental band-origin value of $[A336]_2[UO_2Cl_4]$ in *n*-dodecane. The bands representation is taken from the $[UO_2Cl_4]^{2-}$ frequencies, with details found in Table S2.

Region	E, cm ⁻¹	$\Delta\nu$, cm ⁻¹	I, a.u.	Identification
0	21025.0		7.55E-01	0(0)->1(0)
	20786.3	238.7	2.59E-03	0(0)->1(1 ν_8 , 1 ν_{12})
	20758.9	266.1	1.25E-02	0(0)->1(1 ν_{11})
	20492.7	532.3	2.54E-04	0(0)->1(2 ν_{11})
1	20149.1	875.9	8.88E-02	0(0)->1(1 ν_{14})
	19910.4	238.7	2.93E-04	0(0)->1(1 ν_8 , 1 ν_{12} , 1 ν_{14})
	19883.0	266.1	1.32E-03	0(0)->1(1 ν_{11} , 1 ν_{14})
2	19274.1	875.1	6.75E-03	0(0)->1(2 ν_{14})
	19032.9	241.1	3.44E-05	0(0)->1(1 ν_9 , 1 ν_{12} , 2 ν_{14})
	19007.1	267.0	9.21E-05	0(0)->1(1 ν_{11} , 2 ν_{14})
3	18398.2	875.9	4.07E-04	0(0)->1(3 ν_{14})
	18159.5	238.7	1.26E-06	0(0)->1(1 ν_8 , 1 ν_{12} , 3 ν_{14})
	18132.1	266.1	5.13E-06	0(0)->1(1 ν_{11} , 3 ν_{14})
4	17522.4	875.9	2.11E-05	0(0)->1(4 ν_{14})
	17256.2	266.1	2.48E-07	0(0)->1(1 ν_{11} , 4 ν_{14})

Table S10: Theoretical displacements of geometries ΔR , and absolute frequency shifts $\Delta\nu$ from the ground to the first excited state.

		ΔR , Å		$\Delta\nu$, cm ⁻¹			
		R _{U-O}	R _{U-X}	ν_{U-X}	ν_b	ν_s	ν_a
$[UO_2Cl_4]^{2-}$	gas phase	0.031	0.007	-4	-4	-80	-115
	dodecane	0.031	0.007	1	-1	-78	-106
	acetone	0.03	0.009	-1	-2	-81	-101
$[UO_2Br_4]^{2-}$	gas phase	0.028	0.012	7	2	-31	-53
$[Bu_4N]_2[UO_2Cl_4]$	gas phase	0.026	0.003-0.027	-4	-5	-70	-100
$[A336]_2[UO_2Cl_4]$	gas phase	0.029	0.005-0.021	-5	-4	-74	-103

Supplemental figures

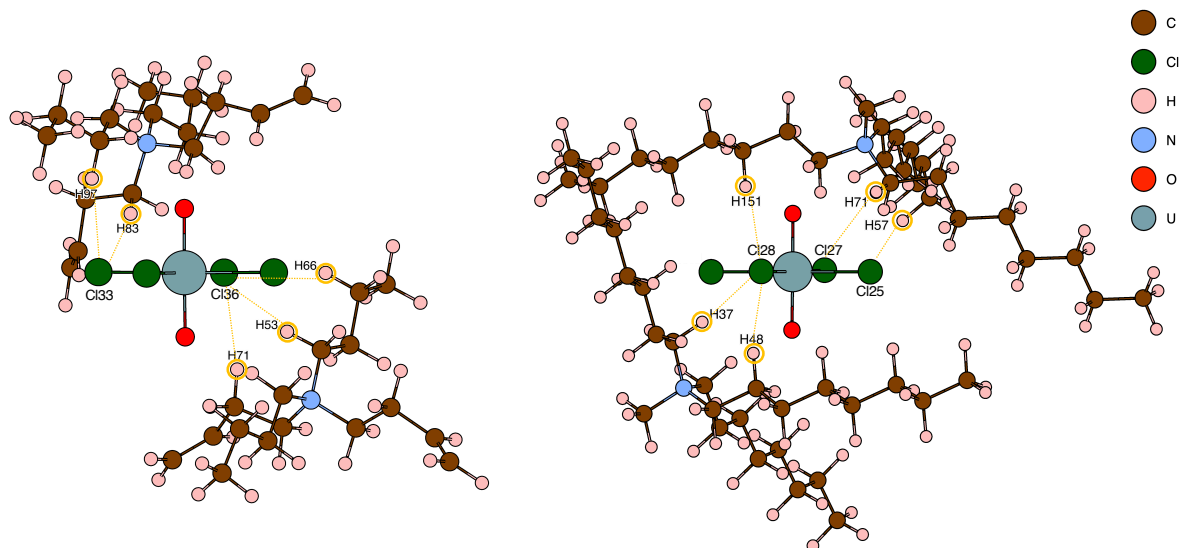


Figure S3: Illustrations of hydrogen bonds between the first and second coordination spheres of uranyl in $[R_4N]_2[UO_2Cl_4]$ complexes. Left panel is representing interactions in $[Bu_4N]_2[UO_2Cl_4]$ and right in $[A336]_2[UO_2Cl_4]$.

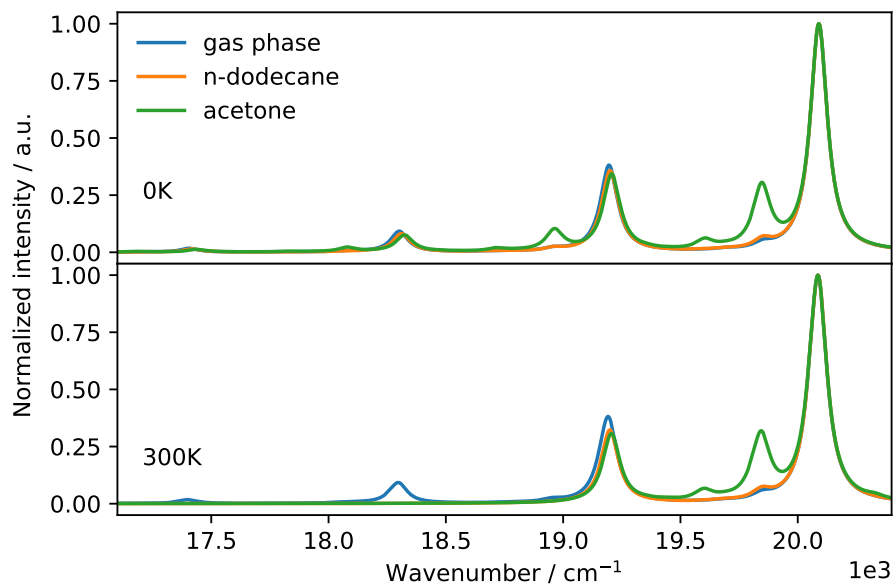


Figure S4: Influence of solvent effects on the theoretical spectrum of $[\text{UO}_2\text{Cl}_4]^{2-}$ at 0 K (upper panel) and 300 K (lower panel). The spectral shapes were obtained by a Lorentzian convolution; the assignments are provided in Tables S4, S5 and S6 for the $[\text{UO}_2\text{Cl}_4]^{2-}$ in gas-phase, *n*-dodecane and acetone, respectively.

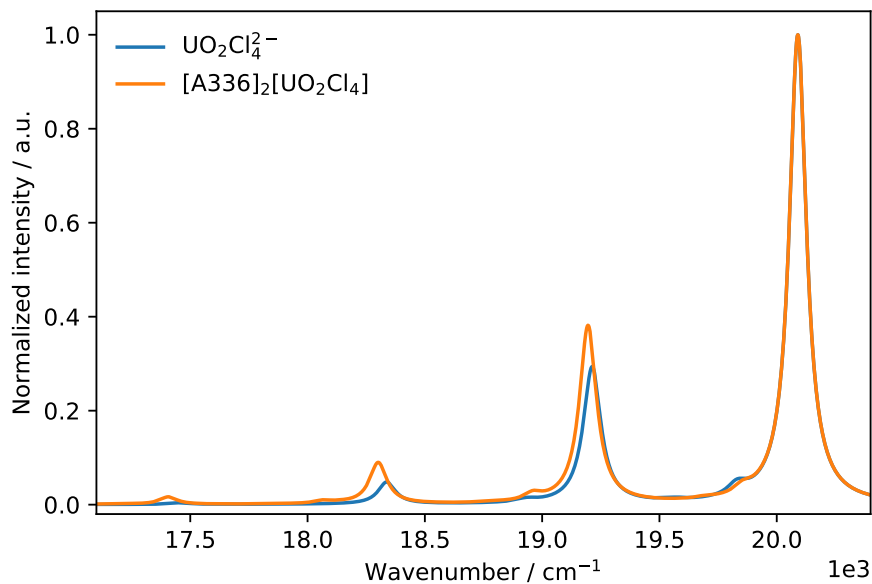


Figure S5: Effect of a $[\text{A336}]^+$ counter ion on the theoretical $[\text{UO}_2\text{Cl}_4]^{2-}$ spectrum in gas-phase at 300 K. The spectral shapes were obtained by a Lorentzian convolution; the assignments are provided in Tables S4 and S9 for the $[\text{UO}_2\text{Cl}_4]^{2-}$ and $[\text{A336}]_2[\text{UO}_2\text{Cl}_4]$, respectively.

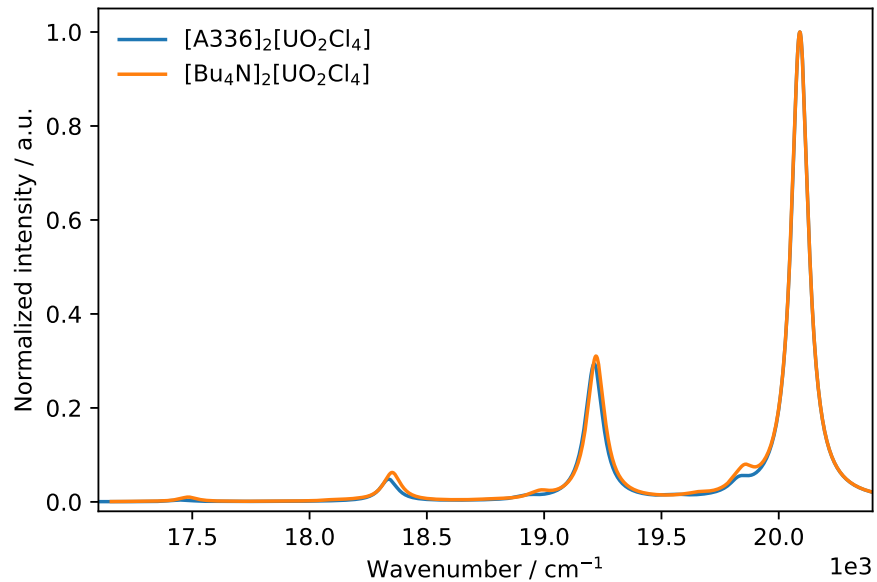


Figure S6: Comparison of the theoretical spectra of $[\text{Bu}_4\text{N}]_2[\text{UO}_2\text{Cl}_4]$ and $[\text{A336}]_2[\text{UO}_2\text{Cl}_4]$ complexes in a gas-phase at 300 K. The spectral shapes were obtained by a Lorentzian convolution; the assignments are provided in Tables S8 and S9 for the $[\text{Bu}_4\text{N}]_2[\text{UO}_2\text{Cl}_4]$ and $[\text{A336}]_2[\text{UO}_2\text{Cl}_4]$, respectively.

Table S11: Cartesian coordinates (in Å) of the $[\text{UO}_2\text{X}_4]^{2-}$ complexes in different media at their ground and first excited state minima obtained by R-ECP DFT/PBE0 and TD-DFT/PBE0 methods, respectively.

$[\text{UO}_2\text{Cl}_4]^{2-}$ gas phase, Turbomole 7.3.1						
	Ground state			Excited state		
Cl	1.919262	1.919262	0	1.9246369	1.9246369	0
Cl	-1.919262	-1.919262	0	-1.9246369	-1.9246369	0
Cl	1.919262	-1.919262	0	1.9246369	-1.9246369	0
Cl	-1.919262	1.919262	0	-1.9246369	1.9246369	0
O	0	0	-1.7581059	0	0	-1.7888649
O	0	0	1.7581059	0	0	1.7888649
U	0	0	0		0 0	0
$[\text{UO}_2\text{Cl}_4]^{2-}$ <i>n</i> -dodecane, G16						
Cl	0	2.698696	0	0	2.706546	0
Cl	0	-2.698696	0	0	-2.706546	0
Cl	-2.698696	0	0	-2.706546	0	0
Cl	2.698696	0	0	2.706546	0	0
O	0	0	1.759301	0	0	1.789492
O	0	0	-1.759301	0	0	-1.789492
U	0	0	0	0	0	0
$[\text{UO}_2\text{Cl}_4]^{2-}$ acetone, G16						
Cl	0	2.683942	0	0	2.691882	0
Cl	0	-2.683942	0	0	-2.691882	0
Cl	-2.683942	0	0	-2.691882	0	0
Cl	2.683942	0	0	2.691882	0	0
O	0	0	1.760965	0	0	1.790628
O	0	0	-1.760965	0	0	-1.790628
U	0	0	0	0	0	0
$[\text{UO}_2\text{Br}_4]^{2-}$ gas phase, Turbomole 7.3.1						
Br	-2.03856600	-2.0385665	0.0000001	-2.0466917	-2.0466919	-0.0001551
Br	2.03856650	2.0385659	0.0000001	2.0466764	2.0466945	-0.0001593
Br	-2.03856600	2.0385658	0	-2.0467227	2.0466596	0.0001346
Br	2.03856600	-2.0385662	0.0000001	2.0466703	-2.0467211	0.0001357
O	-0.00000030	0.0000005	-1.7503044	0.0000395	0.0000376	-1.7775715
O	-0.00000030	0.0000005	1.7503042	0.0000372	0.0000294	1.7776021
U	0.00000010	-0.0000001	-0.0000001	-0.0000091	-0.0000081	0.0000135

Cartesian coordinates in Å of all the complexes

Table S12: Cartesian coordinates (in Å) of the $[\text{Bu}_4\text{N}]_2[\text{UO}_2\text{Cl}_4]$ in gas phase at its ground and first excited state minima obtained in Turbomole 7.3.1 by R-ECP DFT/PBE0 and TD-DFT/PBE0 methods respectively.

	Ground state			Excited state		
C	-1.7231178	2.6706283	-2.6216748	-1.6793731	2.6734267	-2.6465738
C	-2.0317492	1.2075078	-2.8936115	-1.9941509	1.2097959	-2.9084194
C	-3.3758543	1.0920197	-3.5415702	-3.3303708	1.0965456	-3.5728047
C	-4.4133376	0.4600839	-3.0135895	-4.3783182	0.4748322	-3.0534051
C	-0.3096963	4.4588521	-1.8591334	-0.2615627	4.4594906	-1.8864919
C	-0.1792549	2.2495675	-0.7223308	-0.1678411	2.265401	-0.7187768
C	0.7403436	2.4820091	-2.943684	0.7867802	2.4586391	-2.9290301
N	-0.3714943	2.9649229	-2.0406626	-0.3341219	2.9638944	-2.0490737
C	8.2198311	0.6994753	-3.063383	8.1677943	0.7167897	-3.0809801
C	7.1078312	-0.2278135	-3.4509097	7.0503487	-0.2071862	-3.460733
C	6.9992163	-0.8016964	-4.6396134	6.925001	-0.7710549	-4.6525771
C	8.9381358	4.0843228	-4.4134742	8.84534	4.1199889	-4.4064407
C	10.0010406	4.3693995	-5.4735881	9.8818182	4.4204104	-5.4882432
C	0.7639403	3.0479043	-4.346386	0.8343909	3.0027985	-4.3396918
C	1.8951095	2.3959104	-5.1365636	1.9678381	2.3254385	-5.1049056
C	2.0237276	2.9657649	-6.5378999	2.1229064	2.8737564	-6.5121335
C	0.9646197	5.0129345	-1.2460252	1.0009632	5.0091596	-1.2455701
C	0.8803024	6.5064323	-1.2197909	0.939701	6.5038335	-1.2584027
C	0.9391448	7.2434357	-0.120433	0.9678758	7.2674491	-0.1761263
C	-1.173654	2.5638109	0.3729298	-1.1765075	2.6033288	0.3562616
C	-0.8081203	1.7683579	1.624225	-0.8394835	1.822709	1.6246737

Continued on next page

Table S12 – *Continued from previous page*

	Ground state			Excited state		
C	-1.7407864	2.0567479	2.7867969	-1.7907905	2.1336595	2.7661672
C	7.7399134	4.2181381	-1.6440369	7.7130724	4.2168068	-1.6083406
C	8.4885346	5.4138149	-1.0823067	8.4722942	5.4061695	-1.0476814
C	7.5036746	6.4986065	-0.7691173	7.4928854	6.4846622	-0.6976385
C	7.5741331	7.7276482	-1.2582746	7.551544	7.7209691	-1.1697449
C	7.6175083	2.0055634	-2.5780823	7.5738296	2.0153299	-2.5661762
C	9.5478961	3.4588312	-3.1755507	9.486048	3.4809697	-3.1912622
C	9.4345973	2.524316	-0.9564187	9.4275313	2.518378	-0.9822147
C	8.6866428	1.9672626	0.2325169	8.7091061	1.9397153	0.2146703
C	9.65996	1.6011049	1.3469478	9.7073695	1.5752569	1.3073019
C	8.9400933	1.0211657	2.5532241	9.0182853	0.9690792	2.5186037
Cl	5.6570547	3.8447947	1.2252483	5.7037915	3.7874771	1.2948984
Cl	2.6093874	0.1291399	-1.1318178	2.5725988	0.1000307	-1.0465703
Cl	3.9992506	0.5892005	2.413443	3.9935588	0.5548479	2.4965168
Cl	4.2352165	3.317432	-2.1815109	4.2385258	3.2897317	-2.1284497
N	8.5911181	3.0516001	-2.0914457	8.5562295	3.0576174	-2.0899549
O	2.6579787	2.8136216	0.6054672	2.6563163	2.8170192	0.6914103
O	5.5781868	1.0410046	-0.3099148	5.5865699	0.970901	-0.2560554
U	4.1153844	1.9065225	0.1791804	4.1164657	1.8664524	0.2561967
C	11.0137114	5.434966	-5.0831033	10.9007723	5.4842478	-5.1095114
H	-2.4559006	3.0785152	-1.9256472	-2.419443	3.0935144	-1.9657071
H	-1.7982081	3.2485531	-3.5434355	-1.7366446	3.2425793	-3.5750709
H	-1.2748837	0.7780204	-3.5571044	-1.2315038	0.7691541	-3.5577871
H	-2.0215924	0.6273467	-1.968997	-1.9995663	0.6384053	-1.9782886

Continued on next page

Table S12 – *Continued from previous page*

	Ground state			Excited state		
H	-3.4833213	1.5690257	-4.5143349	-3.4222629	1.5658076	-4.5509215
H	-4.3470267	-0.033883	-2.0491824	-4.3275788	-0.0114333	-2.0841513
H	-5.3636916	0.4031782	-3.5307445	-5.3220169	0.418791	-3.5826978
H	-1.1694865	4.7270943	-1.2442715	-1.1354452	4.7457184	-1.3001097
H	-0.4747673	4.889107	-2.8484588	-0.3939071	4.877186	-2.8859806
H	0.8313591	2.485545	-0.3933224	0.840782	2.4954168	-0.3797986
H	-0.1703213	1.1851182	-0.9538556	-0.163531	1.1975964	-0.9348487
H	1.6781943	2.7042229	-2.4331307	1.7199389	2.6815295	-2.409592
H	0.6705955	1.3951138	-2.9564868	0.7084254	1.3722497	-2.9260715
H	8.8870508	0.8395134	-3.9189523	8.8181177	0.8698745	-3.9472294
H	8.8005869	0.2315785	-2.2604406	8.7652978	0.2387174	-2.2964379
H	6.3554238	-0.4110288	-2.6867537	6.3082732	-0.3975701	-2.6882462
H	7.7295906	-0.6321114	-5.4257046	7.6439182	-0.5943258	-5.4475929
H	6.1758188	-1.4679127	-4.8672707	6.0987361	-1.4358077	-4.8740409
H	8.1861272	3.4175562	-4.8417619	8.0844216	3.4567764	-4.8243736
H	8.4286978	5.0183785	-4.1607759	8.3401671	5.0496251	-4.130119
H	10.5203372	3.4386731	-5.7291638	10.3972858	3.4942487	-5.7671456
H	9.4852783	4.6841782	-6.3848823	9.3435881	4.7443912	-6.3831726
H	-0.1819632	2.8781471	-4.8734487	-0.1066389	2.8364979	-4.8766122
H	0.9321954	4.1295991	-4.3262175	1.0160613	4.0824947	-4.3337166
H	2.8304257	2.5281695	-4.5847193	2.8966736	2.4542972	-4.5414708
H	1.7209957	1.3158409	-5.1880289	1.7806363	1.2470119	-5.1436291
H	2.2450226	4.0363524	-6.5097535	2.3576975	3.9417306	-6.4957196
H	1.1029825	2.8320793	-7.1138735	1.2084956	2.7438894	-7.0990188

Continued on next page

Table S12 – *Continued from previous page*

	Ground state			Excited state		
H	2.8306813	2.4769339	-7.0874904	2.9308802	2.3669528	-7.0437125
H	1.8452075	4.7093883	-1.8236081	1.896008	4.677173	-1.7843465
H	1.1193957	4.6333552	-0.2350723	1.1145126	4.6539952	-0.2202624
H	0.7760567	7.0020013	-2.1843963	0.8806151	6.9763318	-2.2382199
H	1.0627443	6.7908448	0.8582337	1.0462638	6.838126	0.8175987
H	0.8916486	8.3253259	-0.1622608	0.9394954	8.3485261	-0.2462526
H	-2.1998613	2.3154108	0.0783695	-2.1995984	2.3587715	0.0481891
H	-1.1602673	3.6301845	0.6214414	-1.1592043	3.6731832	0.5893362
H	0.2246834	1.9950809	1.9040768	0.1897737	2.0454302	1.9203767
H	-0.8252225	0.6989652	1.3896435	-0.8598857	0.7504031	1.4042654
H	-1.7098422	3.1134609	3.0666007	-1.7570608	3.1937903	3.0324141
H	-1.4578685	1.4754306	3.6661139	-1.5285628	1.5620758	3.6581993
H	-2.7777888	1.8077791	2.54197	-2.824966	1.8890225	2.505678
H	7.0416344	3.8371666	-0.8966282	7.0314797	3.8249679	-0.8510347
H	7.1386468	4.5036323	-2.5057393	7.0918112	4.5117038	-2.4524489
H	9.2412281	5.799676	-1.7765467	9.2087551	5.8030053	-1.7531317
H	8.9983067	5.1322407	-0.1544231	9.0029946	5.1135421	-0.1350372
H	6.6948592	6.215431	-0.0989246	6.6991158	6.1899392	-0.0145572
H	8.3714955	8.0315552	-1.9308543	8.3339235	8.0359822	-1.8547064
H	6.8389032	8.4794786	-0.9972636	6.8212509	8.4677866	-0.8818384
H	6.9340373	1.8155002	-1.7513022	6.9086759	1.8163625	-1.7267325
H	7.0229452	2.4744519	-3.3603095	6.9587697	2.4920396	-3.3274802
H	10.2577446	4.1412972	-2.7092372	10.2048478	4.1596966	-2.7332091
H	10.1018386	2.5586908	-3.4467517	10.0359903	2.5860505	-3.4868352

Continued on next page

Table S12 – *Continued from previous page*

Ground state				Excited state		
H	10.0744458	3.3546276	-0.6526366	10.069342	3.3476496	-0.679945
H	10.0864893	1.7656666	-1.3945915	10.0737623	1.7699849	-1.4457339
H	8.1107541	1.0823836	-0.0477573	8.1407886	1.0493279	-0.0645889
H	7.9567762	2.6857104	0.6174913	7.9761006	2.6434691	0.6202086
H	10.2226809	2.4932853	1.6477165	10.2603168	2.4730125	1.6093349
H	10.4011149	0.8825933	0.9745528	10.453713	0.873802	0.9133679
H	8.2046395	1.7265971	2.9456944	8.2763823	1.6565146	2.9304332
H	9.6434408	0.778559	3.3526434	9.7389617	0.7311515	3.3038452
H	8.3999497	0.109224	2.2890534	8.491638	0.0495992	2.2530673
H	11.634522	5.131161	-4.2367324	11.5420253	5.1725295	-4.2814456
H	10.5154962	6.3702383	-4.8128049	10.4066819	6.4149568	-4.8168367
H	11.6894051	5.6503302	-5.9130371	11.5562527	5.7109501	-5.9525399

Table S13: Cartesian coordinates (in Å) of the $[A336]_2[UO_2Cl_4]$ in gas phase at its ground and first excited state minima obtained in Turbomole 7.3.1. by R-ECP DFT/PBE0 and TD-DFT/PBE0 methods respectively.

Ground state				Excited state		
C	-1.6461843	1.2032269	-2.7898103	-1.633078	1.1910779	-2.8057852
C	-0.5220577	3.2945601	-2.294429	-0.532041	3.2905882	-2.295121
C	-0.0115532	1.2329116	-0.9622376	-0.0219215	1.2369558	-0.9570139
C	0.7562838	1.3638802	-3.2560934	0.7708408	1.3704842	-3.2431944
N	-0.3658949	1.7925459	-2.3275443	-0.3642496	1.7906856	-2.3259703
C	8.1975976	1.7276116	-3.1163927	8.164239	1.7028967	-3.134453
C	7.057662	1.1507649	-3.9665424	7.0107299	1.1265578	-3.9654652
C	0.7077407	1.8813497	-4.6808654	0.7500881	1.9200359	-4.6562278

Continued on next page

Table S13 – *Continued from previous page*

	Ground state			Excited state		
C	1.8537649	1.2580073	-5.4787245	1.8757458	1.2730443	-5.4628106
C	1.9286199	1.7585894	-6.9158336	1.9844609	1.814585	-6.8823089
C	0.6900871	4.0531035	-1.797232	0.654431	4.0591905	-1.7525596
C	0.495246	5.5655171	-1.8656286	0.4762728	5.5670984	-1.9064005
C	-0.9271163	1.5988199	0.1906763	-0.979795	1.5620885	0.1731472
C	-0.4031856	0.9528474	1.474797	-0.4617339	0.9389285	1.4703199
C	-1.223735	1.3168107	2.7064365	-1.3267301	1.269012	2.6805805
C	8.2115209	5.2420106	-1.590463	8.217084	5.2184853	-1.6148665
C	9.0401054	6.2481231	-0.8140585	9.063911	6.2190133	-0.851928
C	8.1481801	7.4186072	-0.3968068	8.1873798	7.3976505	-0.4271156
C	7.8496605	3.1628947	-2.7690856	7.8235677	3.1374496	-2.7781333
C	9.9606169	4.360842	-3.0775044	9.9325979	4.3263012	-3.1325281
C	9.5942091	3.2511344	-0.9563462	9.6041048	3.2244248	-1.0023766
C	8.7007022	2.869779	0.204574	8.7341427	2.8461309	0.1769905
C	9.4294255	1.9580388	1.1899717	9.4918775	1.956401	1.1600231
C	8.5778865	1.6647567	2.4210161	8.6678887	1.666431	2.4100975
Cl	5.3884893	4.2984281	0.3064566	5.4510299	4.2706622	0.3366167
Cl	3.2420551	-0.2944559	-1.3911706	3.1912206	-0.3097982	-1.3195414
Cl	4.7608904	0.8807181	1.9952177	4.8012604	0.8545479	2.0403593
Cl	3.985672	3.0256857	-2.8432433	3.9528578	3.0244947	-2.802491
N	8.9204324	3.9995534	-2.0835293	8.9107053	3.9715808	-2.1176084
O	2.7388955	2.4540567	0.1199908	2.7296024	2.4763278	0.1993843
O	5.9502491	1.3823912	-0.8952207	5.9526931	1.3344897	-0.8900281
U	4.3485499	1.9091212	-0.3673548	4.3466912	1.8905967	-0.3161897

Continued on next page

Table S13 – *Continued from previous page*

	Ground state			Excited state		
H	-1.4046432	3.4946698	-1.6658059	-1.4383236	3.4841597	-1.6985912
H	-0.7817986	3.5928913	-3.3225549	-0.7564003	3.5894676	-3.3313615
H	1.012849	1.5669308	-0.7437302	0.9855016	1.605448	-0.7147684
H	0.0389693	0.1413441	-1.096228	0.0756246	0.1487302	-1.0937655
H	1.7025041	1.6699581	-2.784895	1.713517	1.6572178	-2.75183
H	0.7455572	0.2633428	-3.2346128	0.7482958	0.269755	-3.2454746
H	9.1608184	1.6398624	-3.6540545	9.1184122	1.6155065	-3.6882649
H	8.276449	1.1382993	-2.1884052	8.2617595	1.1112358	-2.2091603
H	-0.2528237	1.6494442	-5.1786956	-0.2157256	1.7377552	-5.1651685
H	0.8310311	2.9785813	-4.6943621	0.9167018	3.0116095	-4.6424251
H	2.8019028	1.4814217	-4.957075	2.8268654	1.4427365	-4.9265565
H	1.7477237	0.1563279	-5.4765198	1.7242635	0.1769694	-5.4952025
H	2.0461717	2.8595914	-6.9120747	2.1495802	2.9087937	-6.8417109
H	0.9709829	1.5539303	-7.4348059	1.0227516	1.6691845	-7.4141519
C	3.0737849	1.1344469	-7.7059526	3.1073145	1.1669667	-7.6842936
H	1.588215	3.7853979	-2.3811357	1.5883639	3.7600546	-2.2613403
H	0.9247961	3.769382	-0.7589082	0.8126561	3.822178	-0.68769
H	-1.9691455	1.2705236	0.0164803	-2.001234	1.1874134	-0.0269822
H	-0.9495403	2.6933871	0.3356569	-1.056413	2.6548985	0.3161883
H	0.6484942	1.2578452	1.624974	0.5735104	1.2844171	1.6462799
H	-0.3878051	-0.1466636	1.3526675	-0.3978414	-0.1589915	1.349348
H	-1.2285351	2.4174772	2.8286919	-1.3800557	2.368776	2.801683
C	-0.7000726	0.6728983	3.9854928	-0.8100195	0.64662	3.972517
H	-2.2806273	1.0212465	2.5518233	-2.3666843	0.9309914	2.4992819

Continued on next page

Table S13 – *Continued from previous page*

	Ground state			Excited state		
H	7.3602861	4.8929891	-0.9772772	7.3722848	4.8753488	-0.9888143
H	7.784598	5.7082526	-2.4937803	7.7798279	5.687144	-2.5121589
H	9.8914018	6.6306152	-1.4077287	9.9115202	6.5925165	-1.4568101
H	9.458978	5.7836087	0.0958255	9.4896742	5.7532647	0.0543027
H	6.9730742	3.1678889	-2.1054602	6.9617209	3.1426009	-2.0946294
H	7.5773403	3.7324783	-3.6724679	7.5304103	3.7079881	-3.6745387
H	10.4257158	3.8925993	-0.622177	10.4426746	3.8655498	-0.6849707
H	10.0391224	2.3562154	-1.4185107	10.039784	2.32803	-1.4709907
H	7.7968588	2.3505228	-0.1526226	7.8287635	2.3145072	-0.1580092
H	8.3423506	3.7693938	0.7321074	8.371927	3.7470585	0.6998276
H	10.3930872	2.412322	1.4982492	10.454286	2.4282738	1.4455823
H	9.6845888	1.0062478	0.6840358	9.7530335	1.0018581	0.6619645
H	8.4108146	2.6074578	2.9765874	8.4883168	2.6149005	2.9518627
C	9.1797033	0.6234488	3.3562885	9.3095754	0.6560275	3.3521519
H	7.5745105	1.3288947	2.1009016	7.6666959	1.3038002	2.1127397
H	-1.8902656	1.5901533	-3.7883501	-1.8540593	1.5597719	-3.8167565
H	-2.447729	1.4721236	-2.088683	-2.4516826	1.4706455	-2.128819
H	-1.5395344	0.1093463	-2.8303285	-1.5236557	0.0966638	-2.8244662
H	9.4976102	4.9488504	-3.883417	9.4549004	4.9093163	-3.9337219
H	10.3964441	3.4420853	-3.4938705	10.3615574	3.4052695	-3.551459
H	10.7487221	4.9522443	-2.5917938	10.7293881	4.9208247	-2.6647543
H	-0.7042952	-0.4280191	3.8675313	-0.7662474	-0.453641	3.8553753
C	-1.4954405	1.0499705	5.2301499	-1.6511198	0.9910132	5.1959948
H	0.3602227	0.9565859	4.1253519	0.2342693	0.9728038	4.1390915

Continued on next page

Table S13 – *Continued from previous page*

	Ground state			Excited state		
H	-2.558063	0.7696984	5.0870388	-2.6976975	0.6680509	5.0261044
H	-1.4865368	2.1512956	5.3496641	-1.6903862	2.0919542	5.3145543
C	-0.9738292	0.4033963	6.5092306	-1.1365904	0.3661347	6.488451
H	-0.9830213	-0.6967159	6.3893882	-1.0974087	-0.733508	6.3691767
C	-1.7685197	0.7871262	7.7500482	-1.9777828	0.7166822	7.70804
H	0.0877397	0.6819188	6.6482878	-0.0909875	0.6876049	6.6545314
H	-2.8284367	0.4885377	7.6560217	-3.0220271	0.3750094	7.5872392
H	-1.7460945	1.8790966	7.9178612	-2.004576	1.8087774	7.8755857
H	-1.3642061	0.3023905	8.655625	-1.5775278	0.2488083	8.6243815
C	3.17242	1.6337896	-9.1428483	3.2392894	1.7093182	-9.1024209
H	2.95861	0.0329785	-7.7076248	2.9443251	0.0720774	-7.7238015
H	4.0265774	1.3350572	-7.1795698	4.063717	1.3077747	-7.1448971
H	2.2179737	1.4321839	-9.6682336	2.281857	1.5654449	-9.6415934
C	4.3196435	1.0105598	-9.9313322	4.3666896	1.0665097	-9.9032091
H	3.2885062	2.7355422	-9.1401465	3.4000453	2.8048336	-9.0616359
H	4.2030578	-0.0899241	-9.9325619	4.2064682	-0.0279633	-9.9413383
H	5.271899	1.2112908	-9.4044095	5.3222122	1.2114869	-9.3637366
C	4.4147551	1.5139127	-11.3652394	4.4930493	1.6120298	-11.319002
H	3.4900981	1.2942647	-11.9289699	3.564844	1.4478401	-11.8959722
H	5.2543813	1.0429706	-11.9054404	5.3177593	1.1262492	-11.8692561
H	4.5686073	2.6077455	-11.3964973	4.6899982	2.6995458	-11.3134121
H	0.2481085	5.8688723	-2.9025826	0.3638107	5.8216293	-2.9792051
C	1.7498638	6.3032404	-1.4059537	1.6633694	6.3293623	-1.3256675
H	-0.3685886	5.8693765	-1.2410399	-0.4592259	5.8981767	-1.411689

Continued on next page

Table S13 – *Continued from previous page*

	Ground state			Excited state		
H	2.5997055	5.9897795	-2.0397849	2.5925927	5.9529043	-1.7918052
H	2.0156819	5.9683076	-0.3861392	1.7598216	6.0851677	-0.2510504
C	1.621893	7.821337	-1.4266171	1.5733997	7.840251	-1.4986194
H	1.3468209	8.1576321	-2.4461799	1.5007624	8.0848449	-2.5771766
C	2.8977845	8.5332185	-0.9893175	2.7591406	8.583014	-0.8928346
H	0.7860105	8.132416	-0.7690079	0.635684	8.213194	-1.0400982
H	3.7282081	8.2282757	-1.6554963	3.6961867	8.1925409	-1.3353629
H	3.1832192	8.1797494	0.0201679	2.821807	8.3476725	0.1873177
C	2.7878661	10.0541333	-0.9817578	2.7025212	10.0953551	-1.0779816
H	2.4966596	10.4043774	-1.9908138	2.6465683	10.3285722	-2.1589357
C	4.0723714	10.7513034	-0.5533671	3.8878001	10.8256493	-0.4608366
H	1.9628702	10.3561385	-0.3084341	1.7627083	10.4815597	-0.6382872
H	4.9088156	10.4991218	-1.2304482	4.8424853	10.4837225	-0.9010325
H	4.3726872	10.4469288	0.4655326	3.9464154	10.6449917	0.6278372
H	3.9598992	11.8496994	-0.555265	3.8194902	11.9168783	-0.6154867
H	9.3290653	-0.3217476	2.7981355	9.4714886	-0.295812	2.8086214
C	8.3064351	0.3489486	4.5760302	8.4660173	0.384457	4.5928318
H	10.1879736	0.9461786	3.6862418	10.316117	1.0077915	3.6572149
H	7.2905845	0.0738511	4.234217	7.4502521	0.0795998	4.2762154
H	8.1846111	1.2856827	5.1546271	8.3326027	1.3288745	5.1563825
C	8.8526336	-0.7404977	5.4923957	9.0549707	-0.6743837	5.5181695
H	8.9661239	-1.677251	4.9137407	9.1809585	-1.6188152	4.9544781
C	7.9757058	-1.000942	6.7099023	8.2075473	-0.9331157	6.756523
H	9.8727278	-0.4642193	5.82345	10.0741762	-0.3675641	5.8245524

Continued on next page

Table S13 – *Continued from previous page*

Ground state				Excited state		
H	6.9588529	-1.3095158	6.4082246	7.1932039	-1.2728153	6.4802512
H	7.8734476	-0.092412	7.3306414	8.0935955	-0.015587	7.3620768
H	8.3934291	-1.7983681	7.3494375	8.6568835	-1.7074323	7.4031953
H	7.7335395	7.9032666	-1.3015992	7.7675358	7.8846953	-1.3284139
C	8.871702	8.4612572	0.447091	8.9290822	8.4349345	0.4068213
H	7.2800284	7.0229137	0.1620042	7.3218095	7.010128	0.1416234
H	9.7429557	8.8539358	-0.1133702	9.7990888	8.8172189	-0.1630025
H	9.2841725	7.9759179	1.3527107	9.3456572	7.9478288	1.3098248
C	7.9730432	9.6206695	0.8631596	8.0459906	9.6036712	0.8282279
H	7.5573021	10.1043126	-0.0422156	7.6278218	10.0903772	-0.074816
C	8.6770028	10.669575	1.7162676	8.7688776	10.6455829	1.6734333
H	7.1017052	9.2219058	1.4171583	7.1750414	9.2147353	1.3899872
H	9.5487179	11.0696472	1.1616067	9.6415656	11.0335952	1.1114653
H	9.0912218	10.1860095	2.6226454	9.1843053	10.1582954	2.5774414
C	7.7732165	11.8254896	2.1328072	7.8833334	11.8133195	2.0951097
H	7.3575154	12.3058829	1.2265388	7.4678153	12.2987855	1.191301
C	8.4796916	12.8705764	2.9854278	8.6095237	12.8492746	2.9419921
H	6.9031796	11.4233346	2.6858029	7.0116265	11.4230405	2.6541581
H	9.3334811	13.3182153	2.4452879	9.4660716	13.2847477	2.3959385
H	8.87366	12.4270729	3.9175801	9.0036359	12.4012573	3.8721348
H	7.7970997	13.6904076	3.2687092	7.9404078	13.6789762	3.2292191
H	7.2044857	1.4401424	-5.025524	7.1337586	1.4263597	-5.0247294
H	6.1087275	1.6176728	-3.647695	6.0659397	1.5853394	-3.6227615
C	6.8959417	-0.3599666	-3.8483681	6.8613929	-0.3860122	-3.8574717

Continued on next page

Table S13 – *Continued from previous page*

	Ground state			Excited state		
H	7.7901407	-0.8818376	-4.2444778	7.7466163	-0.898922	-4.2848566
C	5.6364194	-0.8599012	-4.5475215	5.5839534	-0.8858729	-4.52193
H	6.8233575	-0.616522	-2.7755191	6.8226859	-0.654516	-2.7855294
H	5.6968024	-0.6421862	-5.6330947	5.6058445	-0.6500665	-5.6052756
H	4.7775496	-0.2849136	-4.154714	4.734378	-0.3240671	-4.0911763
C	5.3616749	-2.3433383	-4.33576	5.3280228	-2.3745386	-4.3262149
H	6.1998702	-2.9447878	-4.7414065	6.1530055	-2.962998	-4.776036
C	4.0510556	-2.8086398	-4.9614694	3.9958091	-2.8367164	-4.9065779
H	5.3274603	-2.5440842	-3.2482779	5.3398204	-2.5962546	-3.2420462
H	4.0557129	-2.5728676	-6.0439645	3.9554334	-2.5808401	-5.9838837
H	3.2256478	-2.2185758	-4.5197877	3.1860449	-2.2595093	-4.4209165
C	3.7770649	-4.2933944	-4.76372	3.7381282	-4.3263087	-4.7258403
H	4.5722748	-4.9122823	-5.2179134	4.5177204	-4.9322957	-5.22297
H	2.8177685	-4.5957644	-5.220045	2.762759	-4.6261617	-5.1488016
H	3.7320634	-4.5482681	-3.6897659	3.7374553	-4.6016267	-3.6558008